JOURNAL OF PETROLOGY | VOLUME 42 | NUMBER 11 | PAGES 2109–2143 | 2001

Early Proterozoic Calc-Alkaline and Middle Proterozoic Tholeiitic Dyke Swarms from Central–Eastern Argentina: Petrology, Geochemistry, Sr–Nd Isotopes and Tectonic Implications

M. IACUMIN[1,2]*, E. M. PICCIRILLO[1], V. A. V. GIRARDI[3], W. TEIXEIRA[3], G. BELLIENI[4], H. ECHEVESTE[5], R. FERNANDEZ[5], J. P. P. PINESE[6] AND A. RIBOT[7]

[1]DIPARTIMENTO DI SCIENZE DELLA TERRA, UNIVERSITY OF TRIESTE, VIA E. WEISS, 8, 34127 TRIESTE, ITALY

[2]DIPARTIMENTO DI INGEGNERIA CHIMICA, DELL'AMBIENTE E DELLE MATERIE PRIME, UNIVERSITY OF TRIESTE, PIAZZALE EUROPA 1, 34100 TRIESTE, ITALY

[3]INSTITUTO DE GEOCIENCIAS, UNIVERSITY OF SÃO PAULO (USP), PO BOX 11348, 01051 SÃO PAULO, SP, BRAZIL

[4]DIPARTIMENTO DI MINERALOGIA E PETROLOGIA, UNIVERSITY OF PADOVA, CORSO GARIBALDI, 37, 35137 PADOVA, ITALY

[5]INSTITUTO DE RECURSOS MINERALES (FCNyM-UNLP), CALLE 47 N° 522, 1900 LA PLATA, ARGENTINA

[6]DEPARTAMENTO DE GEOCIENCIAS, UNIVERSITY OF LONDRINA, PO BOX 6001, 86051-990 LONDRINA, PR, BRAZIL

[7]LABORATORIO DE ENTRENAMIENTO MULTIDISCIPLINARIO PARA LA INVESTIGACION TECNOLOGICA (LEMIT-CIC and FCNyM-UNLP), PO BOX 128, 1900 LA PLATA, ARGENTINA

RECEIVED JANUARY 2, 2001; REVISED TYPESCRIPT ACCEPTED MAY 11, 2001

The Rio de La Plata craton in Argentina (Azul and Tandil regions) is characterized by Early Proterozoic (2·0 Ga) calc-alkaline and Middle Proterozoic (1·6 Ga) tholeiitic dyke swarms intruding the crystalline basement involved in the Transamazonian Orogeny (2·2–1·9 Ga). The calc-alkaline dykes have andesitic and rhyolitic compositions and trend east–west, whereas the tholeiitic dykes mainly trend N30°W and are represented by basalts with low (0·9–1·7 wt %) and high TiO_2 (up to 3·7 wt %). The calc-alkaline dykes have primitive mantle (PM)-normalized trace element patterns enriched in Rb, Ba, K, La, Ce and Nd, and significant negative Nb and Ti anomalies. These dykes are characterized by $\varepsilon^t(Nd)$ values of −3 to −4, similar to those of the EMI mantle component. Low-TiO_2 tholeiitic dykes have low incompatible-element (IE) contents and PM-IE patterns with slightly positive or negative Nb spikes. They have variable $\varepsilon^t(Nd)$ values (−0·5 to 12·1), which mainly reflect derivation from a depleted source mantle. High-TiO_2 tholeiitic dykes have more enriched IE-PM patterns and are characterized by $\varepsilon^t(Nd)$ values (−1·4 to −7·5) typical of an enriched source mantle. Chemical and isotopic data and melting modelling indicate that both calc-alkaline and tholeiitic dykes originated by different melting degrees of a heterogeneous source mantle, the variable IE enrichment of which may have occurred in Late Archaean to Early Proterozoic times. The emplacement of the calc-alkaline dykes is associated with the transtensional stage of the Transamazonian Orogeny, whereas the tholeiitic dykes reflect extensional tectonics succeeding the Transamazonian event. The calc-alkaline and tholeiitic dykes are similar in emplacement age and characteristics to metamorphosed granites and volcanic rocks outcropping within the

*Corresponding author. Present address: Dipartimento di Scienze della Terra, University of Trieste, Via E. Weiss, 8, 34127 Trieste, Italy. Fax: 0039-040-6762213. E-mail: jacumin@univ.trieste.it

Namaqua fold belts of southwestern Africa (Richtersveld and Witberg–Aggeneys–Gamsberg provinces); this may indicate that the Rio de La Plata craton and southwestern Africa were contiguous in Early–Middle Proterozoic times.

KEY WORDS: *Argentina; geochemistry; petrology; Proterozoic dykes; Rio de La Plata craton*

INTRODUCTION

Precambrian dyke swarms are common in cratonic blocks, providing useful correlations between different tectonic units and yielding information on related geodynamic processes (Halls, 1987; Parker *et al.*, 1990; Baer & Heimann, 1995).

The crystalline basement of the Azul and Tandil regions (Buenos Aires province, Argentina; Fig. 1) belongs to the Rio de La Plata craton and is intruded by unmetamorphosed Proterozoic mafic, intermediate and felsic dyke swarms of 2·0 and 1·6 Ga age, respectively (Teixeira *et al.*, in preparation). Similarly, the portion of the Rio de La Plata craton in Uruguay is characterized by unmetamorphosed Proterozoic dyke swarms (Fig. 1) dated at 1·7 Ga (Florida region; Bossi *et al.*, 1993; Teixeira *et al.*, 1999) and ~0·7 Ga (Nico Perez and Treinta y Tres regions; Mazzucchelli *et al.*, 1995; Rivalenti *et al.*, 1995; Girardi *et al.*, 1996).

Study of the Argentinian dykes is important for an understanding of source mantle characteristics in Early–Middle Proterozoic times, as well as for better insight into the processes responsible for craton stabilization in the southernmost part of the South American platform.

In this paper we characterize the Proterozoic calc-alkaline and tholeiitic dyke swarms of central–eastern Argentina in terms of petrological and genetic implications, and relationships between tectonics and magmatism. We show that these dyke swarms originated from depleted- to incompatible element-enriched mantle sources, and that their emplacement occurred during the transtensional to post-collisional stages of the Transamazonian Orogeny (2·2–1·9 Ga).

GEOLOGICAL FRAMEWORK AND DYKE OCCURRENCE

The southernmost Archaean–Proterozoic cratonic areas of South America (Fig. 1) are exposed in Uruguay

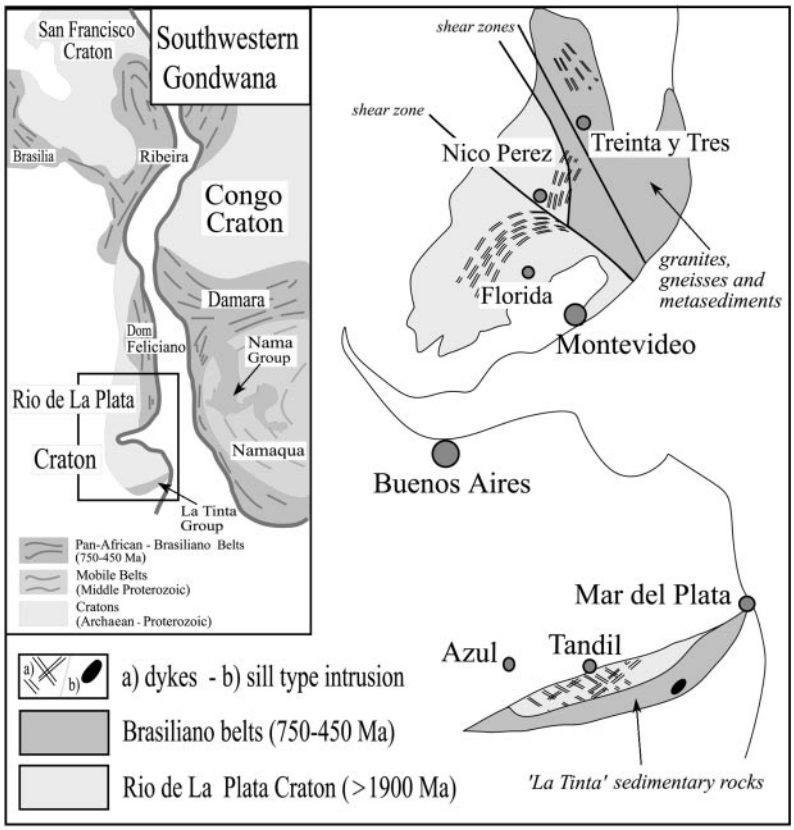

Fig. 1. Simplified geological sketch map of NE Argentina (Dalla Salda *et al.*, 1988) and Uruguay (Mazzucchelli *et al.*, 1995) showing Precambrian dyke occurrences. Inset: Pre-Atlantic South America–South Africa configuration modified after Trompette (1994).

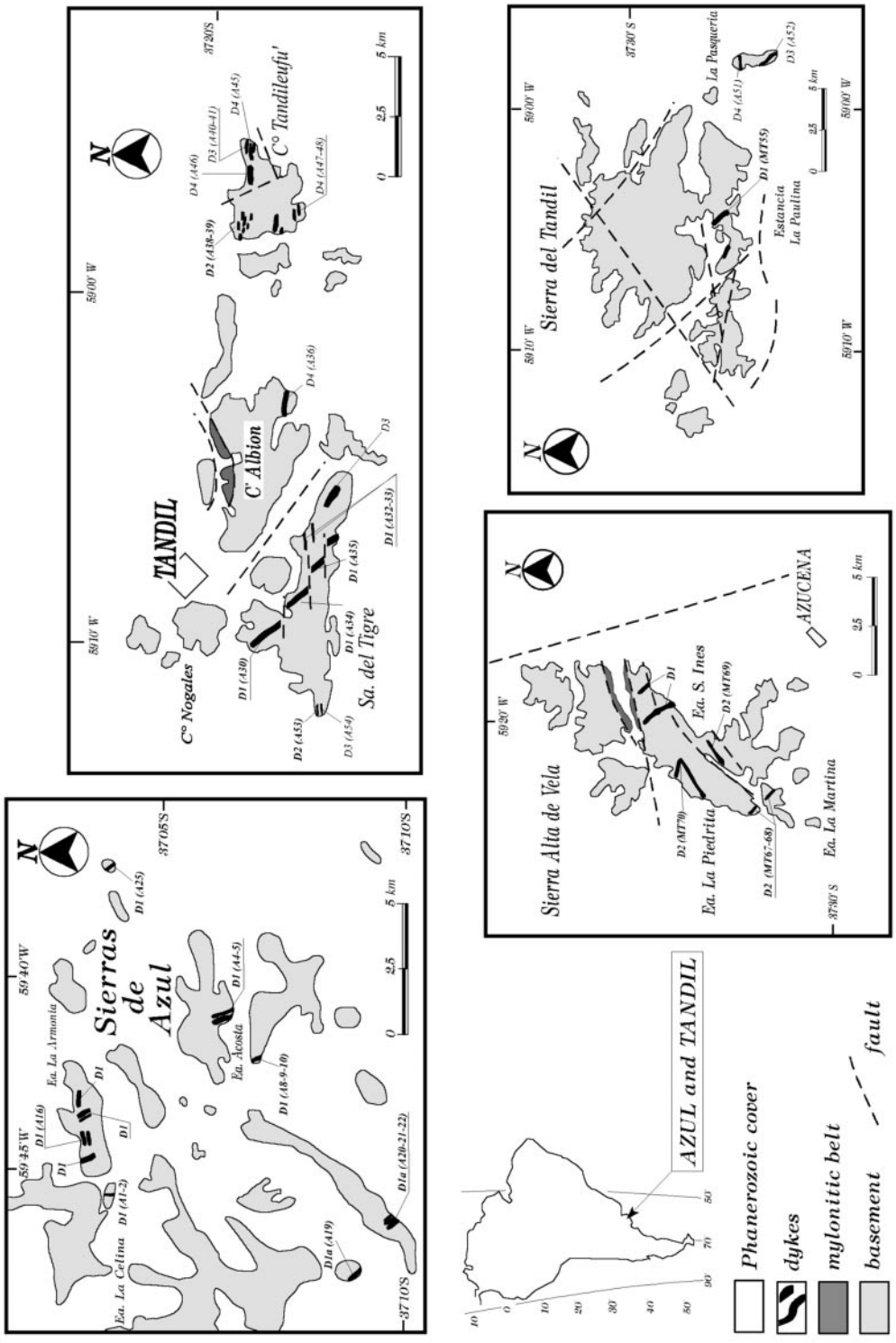

Fig. 2. Simplified geological sketch map of dyke occurrences in Azul and Tandil regions (Argentina). D1, D1a, D2, tholeiitic basalts and basaltic andesites, respectively; D3, D4, calc-alkaline basaltic andesites, andesites, and rhyolites, respectively. Sample numbers in parentheses (see also Table 5).

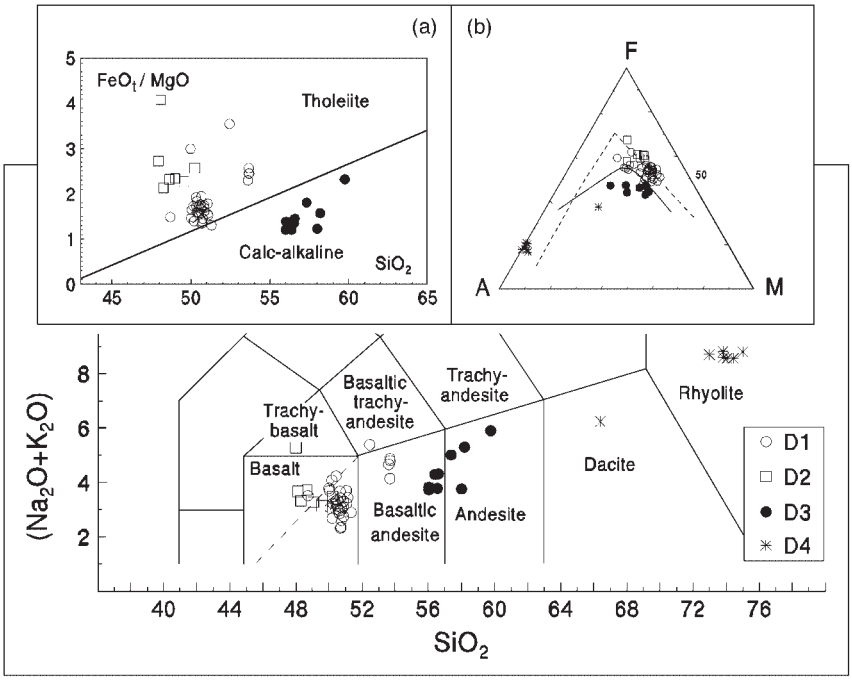

Fig. 3. Classification diagrams of the Azul and Tandil dyke swarms in terms of TAS (Zanettin, 1984; Le Bas *et al.*, 1986), SiO_2 vs Fe_t/MgO (Miyashiro, 1974) and AFM: continuous curve (calc-alkaline–tholeiitic boundary) after Irvine & Baragar (1971); dashed curve (tholeiitic trend) after Macdonald & Katsura (1964). D1, D2, tholeiitic suite; D3, D4, calc-alkaline suites.

Table 1: Plagioclase microprobe compositions of tholeiitic (D1) and calc-alkaline (D3) dykes from the Azul and Tandil regions

Rock:	ThB	ThB		ThB	ThB	BAnd	ThB	ThB	And
Group:	D1	D1		D1	D1	D1	D1	D1	D3
Sample:	A2	A5		A8	A16	A19	A25	A34	A54
Plagioclase:	r	c1	c2	r	r	c	r	r	r
SiO_2	52·83	50·28	55·40	53·66	50·98	53·21	53·32	51·07	59·89
TiO_2	0·05	0·05	0·05	0·06	0·04	0·06	0·12	0·04	
Al_2O_3	30·01	31·59	28·30	29·06	31·05	29·85	29·26	29·85	25·30
FeO_{tot}	0·76	0·60	0·46	0·58	0·76	0·28	0·98	1·51	
CaO	12·43	14·33	10·42	11·45	13·72	12·22	11·70	12·71	6·90
Na_2O	4·43	3·35	5·64	4·95	3·53	4·35	4·84	2·43	7·75
K_2O	0·12	0·02	0·08	0·10	0·27	0·47	0·04	2·54	0·02
Total	100·63	100·22	100·35	99·86	100·35	100·44	100·26	100·15	99·86
Or (wt %)	0·71	0·12	0·46	0·58	1·63	2·75	0·23	15·24	0·12
Ab (wt %)	37·53	28·49	47·77	42·17	30·02	36·72	41·24	20·82	65·61
An (wt %)	61·76	71·40	51·78	57·26	68·36	60·53	58·53	63·94	34·27

ThB, tholeiitic basalt; BAnd, basaltic andesite; And, andesite; FeO_{tot}, total Fe as FeO; c, core; r, rim.

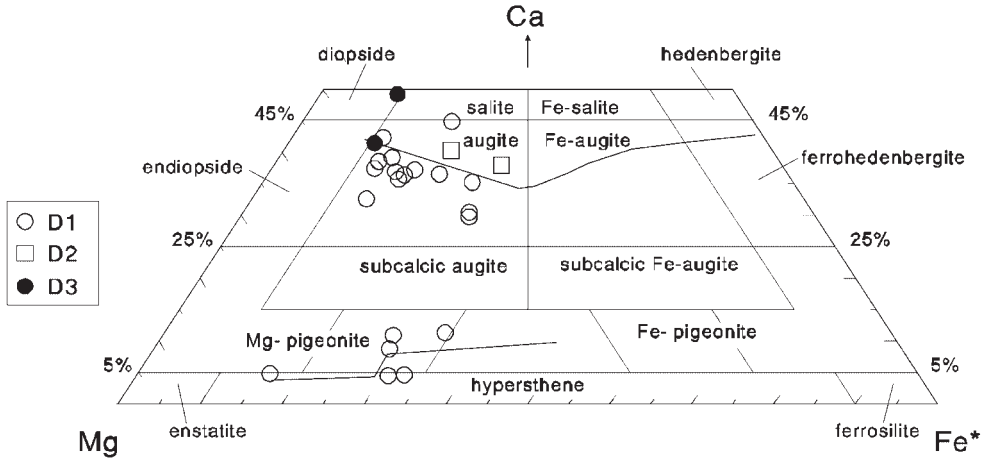

Fig. 4. Ca-rich and Ca-poor pyroxenes of Azul and Tandil basic–intermediate dyke swarms. Continuous curves, Skaergaard trends. ○, □ and ●, D1, D2 (tholeiitic) and D3 (calc-alkaline) dykes, respectively. Fe* = Fe^{2+} + Mn + Fe^{3+}.

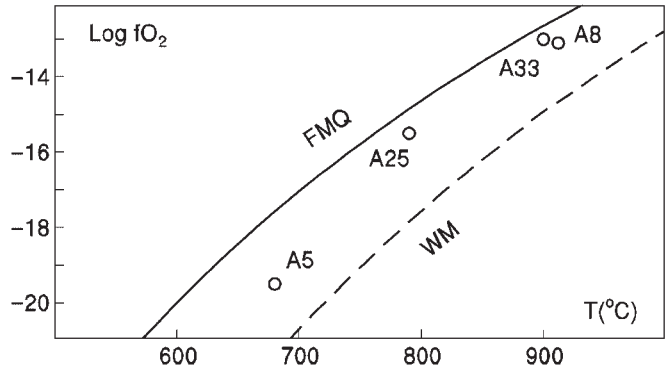

Fig. 5. Log(fO_2) vs T (°C) for homogeneous magnetite–ilmenite pairs from D1 tholeiitic dykes. FMQ, fayalite–magnetite–quartz; WM, wüstite–magnetite.

and Argentina (Azul and Tandil regions) and belong to the Rio de La Plata craton, characterized by terranes involved in the tectonic–metamorphic and magmatic events of the Transamazonian Orogeny (2·2–1·9 Ga) and the Brasiliano cycle (0·8–0·5 Ga). The Rio de La Plata crystalline basement is mainly composed of gneisses, migmatite and granitoids. The Precambrian unmetamorphosed dyke swarms in Uruguay (Fig. 1; Bossi *et al.*, 1993; Mazzucchelli *et al.*, 1995; Rivalenti *et al.*, 1995; Girardi *et al.*, 1996) intrude the crystalline terranes affected by both Transamazonian and Brasiliano events, and are dated as Early and Late Proterozoic, respectively: Florida 1·73 and 1·77 Ga (Teixeira *et al.*, 1999) and Nico Perez and Treinta y Tres 0·7–0·6 Ga (Mazzucchelli *et al.*, 1995; Rivalenti *et al.*, 1995; Girardi *et al.*, 1996). In contrast, the Precambrian unmetamorphosed dyke swarms in Argentina intrude exclusively crystalline terranes of the Rio de La Plata craton and are dated at 2·0 Ga and 1·6 Ga (biotite $^{40}Ar/^{39}Ar$ and baddeleyite U–Pb ages, respectively; Teixeira *et al.*, in preparation). It is also noted that the Late Proterozoic sedimentary rocks of the Argentina 'La Tinta Group' (0·8–0·5 Ga, Fig. 1) in the southern Azul–Tandil regions are locally (Sierra de Los Barrientos) intruded by tholeiitic sills (0·5 Ga; Rapela *et al.*, 1974).

The stratigraphy of the Azul and Tandil regions (Fig. 2) is not well constrained in terms of radiometric ages. The oldest rocks are gneisses, migmatites, mica-schists and medium-grade amphibolites (Teruggi *et al.*, 1974). They are intruded by granitoid bodies whose Rb/Sr ages cluster around 2·2–2·0 and 1·8–1·6 Ga (Varela *et al.*, 1988; Dalla Salda *et al.*, 1992). The 'old granitoids' (gabbroic to granitic rocks) outcrop in the northern part of the 'Azul and Tandil Sierras'; the 'young granitoids' (mainly monzogranites) are located in the southern part of these 'Sierras'. The emplacement of both 'old' and 'young' granitoids has been related to the syn/late- to post-collisional stages, respectively, of the Transamazonian Orogeny (Varela *et al.*, 1985,

Table 2: Ca-rich (cpx) and Ca-poor (pig and opx) pyroxene microprobe compositions of the tholeiitic (D1, D1a and D2) and calc-alkaline (D3) dykes from the Azul and Tandil regions

Rock:	ThB		ThB		ThB			ThB		ThB			
Group:	D1		D1		D1			D1		D1			
Sample:	A2		A5		A8			A16		A25			
Pyroxene:	cpx/c	cpx/r	cpx/c	cpx/r	cpx/c	cpx/r	pig/r	cpx/r	opx/r	cpx/c	cpx/r	opx/c	opx/r
SiO_2	50·99	51·09	52·57	50·34	52·94	52·41	53·52	52·16	55·37	52·13	51·57	53·03	52·29
TiO_2	0·49	0·55	0·09	0·70	0·34	0·46	0·23	0·42	0·12	0·52	0·57	0·30	0·39
Al_2O_3	4·46	1·94	0·35	1·69	2·20	1·91	0·97	3·59	2·71	2·07	2·19	0·94	1·44
FeO_{tot}	6·78	16·53	11·40	15·49	7·80	10·15	17·90	9·37	10·42	10·87	12·84	19·31	20·22
MnO	0·16	0·42	0·21	0·37	0·20	0·21	0·41	0·25	0·20	0·27	0·28	0·37	0·47
MgO	16·06	14·43	13·09	13·58	17·59	17·02	22·32	16·65	29·23	16·05	14·92	23·30	22·36
CaO	20·31	14·60	22·18	16·99	19·22	17·65	4·33	17·93	2·47	18·36	17·83	2·27	2·31
Na_2O	0·28	0·17	0·13	0·24	0·23	0·25	0·07	0·21	0·04	0·18	0·23	0·01	0·05
Cr_2O_3	0·58	0·00	0·00	0·00	0·24	0·08	0·02	0·09	0·35	0·03	0·04	0·10	0·05
Total	100·10	99·74	100·02	99·40	100·76	100·14	99·77	100·67	100·91	100·48	100·47	99·63	99·58
Fe_2O_3*	1·61	0·69	0·68	1·87	1·58	1·56	0·00	0·55	0·00	1·47	1·63	0·55	0·96
Si	1·869	1·937	1·981	1·919	1·926	1·932	1·977	1·910	1·940	1·926	1·921	1·962	1·945
Al(IV)	0·131	0·063	0·015	0·076	0·074	0·068	0·023	0·090	0·060	0·074	0·079	0·038	0·055
Total	2·000	2·000	1·996	1·995	2·000	2·000	2·000	2·000	2·000	2·000	2·000	2·000	2·000
Al(VI)	0·062	0·024	0·000	0·000	0·020	0·015	0·019	0·065	0·052	0·016	0·017	0·003	0·008
Fe^{2+}	0·163	0·504	0·340	0·440	0·194	0·270	0·553	0·272	0·305	0·295	0·354	0·582	0·602
Fe^{3+}	0·044	0·020	0·019	0·054	0·043	0·043	0·000	0·015	0·000	0·041	0·046	0·015	0·027
Cr	0·017	0·000	0·000	0·000	0·007	0·002	0·001	0·003	0·010	0·001	0·001	0·003	0·001
Mg	0·878	0·816	0·735	0·772	0·954	0·935	1·229	0·909	1·526	0·884	0·829	1·285	1·240
Mn	0·005	0·013	0·007	0·012	0·006	0·007	0·013	0·008	0·006	0·009	0·009	0·012	0·015
Ti	0·013	0·016	0·003	0·020	0·009	0·013	0·006	0·011	0·003	0·015	0·016	0·008	0·011
Ca	0·798	0·593	0·895	0·694	0·749	0·697	0·171	0·703	0·093	0·727	0·712	0·090	0·092
Na	0·020	0·013	0·009	0·018	0·016	0·018	0·005	0·015	0·003	0·013	0·017	0·001	0·004
Total	2·000	1·999	2·008	2·010	1·998	2·000	1·997	2·001	1·998	2·001	2·001	1·999	2·000
Ca	42·27	30·47	44·84	35·19	38·49	35·71	8·70	36·86	4·82	37·17	36·51	4·54	4·66
Mg	46·50	41·93	36·82	39·15	49·02	47·90	62·51	47·67	79·07	45·19	42·51	64·77	62·75
Fe†	11·23	27·60	18·34	25·66	12·49	16·39	28·79	15·47	16·11	17·64	20·97	30·70	32·59

1988; Dalla Salda *et al.*, 1992). Mylonitic belts associated with the 'old granitoids' (Fig. 2) may reflect wrench or overthrusting tectonics (Dalla Salda, 1981; Ramos *et al.*, 1990; Dalla Salda *et al.*, 1992).

The southern parts of the Azul and Tandil 'Sierras' are covered by Late Proterozoic sedimentary rocks of the 'La Tinta Group' (up to 400 m thick). These rocks correspond to those of the 'Nama Group' in South Africa (Fig. 1), suggesting a common sedimentary basin origin (Dalla Salda, 1982; Kawashita *et al.*, 1999).

The unmetamorphosed dykes studied here intrude the crystalline basement terranes and the 'old' and 'young granitoids', and mainly strike N30°W in Azul, and N30°W and east–west in Tandil. The dykes (Fig. 2) are divided into two main groups according to field and chemical features (see below). The dykes of the first group (D1 and D2) mainly trend N30°W and have tholeiitic characteristics; those of the second group (D3 and D4) have an east–west strike and a calc-alkaline signature (see Fernandez & Echeveste, 1995).

Most of the tholeiitic dykes are low in TiO_2 (<1·7 wt %, D1), although a few have TiO_2 up to 3·7 wt % (D2). D1 dykes occur in both the Azul and Tandil 'Sierras', are subvertical, vary in thickness from 10 to 50 m, and extend for distances of up to 5 km. They are fine grained at the border and coarse grained

Rock:	ThB		ThB		BAnd			Trb		BAnd	
Group:	D1		D1		D1a			D2		D3	
Sample:	A33		A34		A19			A38		A41	
Pyroxene:	cpx/c	cpx/r	cpx/c	cpx/r	cpx/r	pig/c	pig/r	cpx/c	cpx/r	cpx/c	cpx/r
SiO_2	52·05	51·85	52·29	53·26	51·76	53·32	52·44	51·06	49·38	54·03	52·89
TiO_2	0·42	0·47	0·25	0·25	0·45	0·19	0·34	1·25	1·39	0·05	0·34
Al_2O_3	2·71	2·39	2·88	1·78	1·23	1·05	1·00	2·27	2·89	0·29	2·04
FeO_{tot}	8·41	10·18	7·73	8·83	17·17	17·37	20·79	12·38	16·16	5·88	6·51
MnO	0·26	0·29	0·13	0·17	0·34	0·47	0·52	0·36	0·42	0·21	0·14
MgO	16·60	16·44	17·50	19·20	14·82	21·70	19·02	13·62	11·45	14·78	16·80
CaO	19·25	17·75	18·19	16·30	14·50	5·38	5·48	19·43	17·62	24·45	20·20
Na_2O	0·25	0·21	0·21	0·15	0·11	0·02	0·07	0·23	0·17	0·26	0·23
Cr_2O_3	0·21	0·12	0·04	0·18	0·04	0·07	0·00	0·14	0·08	0·33	0·50
Total	100·16	99·70	99·22	100·12	100·42	99·57	99·66	100·74	99·56	100·28	99·65
Fe_2O_3*	1·61	1·19	0·66	1·00	0·83	0·00	0·00	0·91	0·08	0·34	0·00
Si	1·913	1·924	1·928	1·944	1·952	1·976	1·975	1·908	1·898	1·992	1·947
Al(IV)	0·087	0·076	0·072	0·056	0·048	0·024	0·025	0·092	0·102	0·008	0·053
Total	2·000	2·000	2·000	2·000	2·000	2·000	2·000	2·000	2·000	2·000	2·000
Al(VI)	0·030	0·029	0·053	0·021	0·007	0·022	0·019	0·008	0·029	0·005	0·036
Fe^{2+}	0·214	0·283	0·220	0·242	0·518	0·538	0·655	0·361	0·517	0·172	0·200
Fe^{3+}	0·045	0·033	0·018	0·028	0·024	0·000	0·000	0·026	0·002	0·009	
Cr	0·006	0·004	0·001	0·005	0·001	0·002	0·000	0·004	0·002	0·010	0·014
Mg	0·910	0·909	0·962	1·045	0·833	1·199	1·068	0·759	0·656	0·812	0·922
Mn	0·008	0·009	0·004	0·005	0·011	0·015	0·017	0·012	0·014	0·006	0·004
Ti	0·012	0·013	0·007	0·007	0·013	0·005	0·010	0·035	0·040	0·001	0·009
Ca	0·758	0·706	0·719	0·638	0·586	0·214	0·221	0·778	0·726	0·966	0·797
Na	0·018	0·015	0·015	0·010	0·008	0·001	0·005	0·017	0·013	0·019	0·016
Total	2·001	2·001	1·999	2·001	2·001	1·996	1·995	2·000	1·999	2·000	1·998
Ca	39·17	36·39	37·39	32·58	29·72	10·89	11·27	40·19	37·91	49·16	41·45
Mg	47·03	46·86	50·03	53·37	42·24	60·99	54·46	39·20	34·26	41·32	47·95
Fe†	13·80	16·75	12·58	14·04	28·04	28·13	34·27	20·61	27·83	9·52	10·61

Fe_2O_3* calculated according to Papike *et al.* (1974). Abbreviations as in Table 1, and Trb, trachybasalt. Fe† is Fe^{2+} + Mn + Fe^{3+}.

in the centre. D2 dykes are exposed only in the Tandil 'Sierras', are subvertical, and trend east–west in the 'Don Pedro' quarry (Cerro Tandileufú) and in the southwestern part of the 'Sierra del Tigre', and NW–SE and ~NE–SW in the 'Sierra Alta de Vela'. D2 dykes vary in thickness from 0·5 to 10 m and are medium to fine grained.

The calc-alkaline dykes have andesitic (D3) and rhyolitic (D4) composition. D3 dykes outcrop in the Tandil 'Sierras', mostly along the belt comprising Sierra del Tigre, Cerro Albion and Cerro Tandileufú. These dykes, 0·5–10 m thick, strike east–west, are vertical to moderately inclined (45°S), and have a medium–fine texture. D4 rhyolitic dykes are associated with, and sometimes intruded by, D3 dykes (Tandileufú quarry). D4 dykes strike east–west, are subvertical, and may reach 30 m in thickness (Brigitte quarry).

CLASSIFICATION, PETROGRAPHY AND MINERAL CHEMISTRY

Total alkalis–SiO_2 (TAS) and total alkalis–total Fe–MgO (AFM) diagrams (Fig. 3) reveal that dykes with SiO_2 <54 wt % (D1 and D2) are characterized by pronounced FeO_{tot} enrichment and straddle the tholeiitic trend of

Table 3: Olivine microprobe compositions of tholeiitic (D1) dykes from the Azul and Tandil regions

Rock:	ThB			ThB			
Sample:	A5			A34			
Group:	D1			D1			
Olivine:	c1	c2	r2	c1	r1	c2	r2
SiO_2	36·56	37·40	36·68	38·99	38·75	38·79	39·07
Al_2O_3	0·00	0·00	0·01	0·03	0·04	0·05	0·00
FeO_{tot}	31·77	28·14	30·77	20·12	20·29	20·60	20·02
MnO	0·40	0·37	0·41	0·39	0·32	0·30	0·19
MgO	31·18	33·66	32·16	40·94	40·47	40·50	40·56
CaO	0·22	0·28	0·17	0·26	0·33	0·26	0·25
Total	100·12	99·85	100·20	100·73	100·20	100·50	100·09
Si	0·997	1·003	0·994	0·996	0·997	0·996	1·003
Al(IV)	0·000	0·000	0·000	0·001	0·001	0·001	0·000
Total	0·997	1·003	0·994	0·997	0·998	0·997	1·003
Fe^{2+}	0·724	0·631	0·698	0·430	0·436	0·442	0·430
Mn	0·009	0·009	0·010	0·008	0·007	0·007	0·004
Mg	1·267	1·346	1·299	1·560	1·552	1·550	1·552
Ca	0·006	0·008	0·005	0·007	0·009	0·007	0·007
Total	2·006	1·994	2·012	2·005	2·004	2·006	1·993
Fo	63·63	68·08	65·07	78·39	78·05	77·80	78·32
Fa	36·37	31·92	34·93	21·61	21·95	22·20	21·68

Abbreviations as in Table 1. Fo, forsterite; Fa, fayalite.

Hawaii (Macdonald & Katsura, 1964); dykes with SiO_2 >56 wt % (D3 and D4) plot in the calc-alkaline field of Irvine & Baragar (1971) (Fig. 3b). These data and the SiO_2–(FeO_{tot}/MgO) relationships (Fig. 3a) indicate that the Azul–Tandil dykes belong to different magmatic suites with tholeiitic and calc-alkaline characteristics, respectively.

The dykes of the tholeiitic suite mainly correspond to basalts and basaltic andesites, the high-TiO_2 (HTi) samples (D2) having lower SiO_2 and higher incompatible element abundances (see below) than the low-TiO_2 (LTi) analogues (D1). The dykes of the calc-alkaline suite plot in the fields of basaltic andesite and andesite (D3), and in those of dacite and rhyolite (D4).

LTi tholeiitic dykes (D1) have a subophitic texture dominated by plagioclase (Table 1) and pyroxenes (Table 2). Plagioclase is labradoritic ($An_{71–52}$) and may be altered to clay minerals and sericite. Augite (Wo = 42–30), often associated with orthopyroxene (Wo = 4·5–4·8) or pigeonite (Wo = 8·7–11·3), has total compositional variations that mimic those of the Skaergaard intrusion (Fig. 4). The TiO_2 content of augites is low and ranges from 0·25 to 0·70 wt %. Pyroxenes may be partly or completely replaced by hornblende, tremolite and chlorite. In general, olivine is scarce and restricted to low-Ca pyroxene-free samples. Olivine phenocryst compositions (Table 3) are either virtually constant (sample A34, Fo = 77·8–78·4%) or have a small range (sample A5) from 63·6 to 68·1%. The forsterite content of tholeiitic basalt A34 is in equilibrium ($K_{dFe\text{-}Mg}$ = 0·30; Takahashi & Kushiro, 1983) with the bulk-rock composition {100 × [at. Mg/(Mg + Fe^{2+})], *mg*-number = 51·3}, whereas this is not the case for the olivine of tholeiitic basalt A5 (*mg*-number = 60·2), which would require equilibrium olivine with Fo = 83%. Magnetite (ulvöspinel 26–63%) and ilmenite (R_2O_3 2·3–9·4%) are usually confined to the groundmass (Table 4). Quartz, apatite and epidote are common accessory phases. The crystallization temperatures (Kretz, 1982) of D1 pyroxenes range from 1130 to 1205°C, with Cpx–Opx equilibration at 1121°C (Iacumin, 1998). According to the Loucks (1996) thermometer, the olivine–augite equilibrium temperature for sample A34 is ~1165°C. The homogeneous magnetite–ilmenite pairs yielded subsolidus equilibration temperatures ranging from 680 to 900°C

Table 4: Magnetite and ilmenite microprobe compositions of tholeiitic (D1, D1a, D2) and calc-alkaline (D3, D4) dykes from the Azul and Tandil regions

Rock:	ThB	ThB	ThB	ThB	ThB	ThB	ThB	
Sample:	A5	A8	A25	A33	A34	A2	A16	
Group:	D1	D1	D1	D1	D1	D1	D1	
Magnetite								
SiO_2	0·10	0·13	0·25	0·03	0·26	0·11	0·03	
TiO_2	15·42	21·78	15·78	19·12	9·03	9·69	10·74	
Al_2O_3	1·71	2·23	1·79	2·86	1·80	1·63	0·80	
FeO_{tot}	77·59	71·76	72·28	74·64	84·50	84·67	84·41	
MnO	0·67	0·02	0·46	0·00	0·14	0·02	0·43	
MgO	0·04	0·04	0·54	0·00	0·29	0·00	0·05	
CaO	0·02	0·16	5·78	0·14	0·76	0·12	0·07	
Cr_2O_3	0·04	0·00	0·05	0·03	0·00	0·18	0·04	
Total	95·59	96·12	96·93	96·82	96·78	96·42	96·57	
FeO	44·81	51·08	38·38	49·09	39·17	40·72	41·03	
Fe_2O_3	36·42	22·97	37·67	28·38	50·37	48·83	48·19	
Total*	99·23	98·42	100·71	99·66	101·82	101·30	101·39	
% Ulv.	44·83	63·41	44·87	54·94	26·40	27·95	30·51	
Rock:	ThB	ThB	ThB	ThB	BAnd	Trb	BAnd	Dacite
Sample:	A5	A8	A25	A33	A19	A38	A41	A36
Group:	D1	D1	D1	D1	D1a	D2	D3	D4
Ilmenite								
SiO_2	0·07	0·25	0·01	0·05	0·01	0·06	0·24	0·25
TiO_2	50·83	49·91	50·04	49·32	50·62	50·50	48·13	48·91
Al_2O_3	0·00	0·05	0·02	0·36	0·02	0·07	0·22	0·18
FeO_{tot}	45·75	44·98	46·87	45·30	46·20	45·96	39·73	41·95
MnO	1·95	2·68	2·10	3·70	1·46	2·39	4·75	6·25
MgO	0·00	0·07	0·03	0·07	0·05	0·00	0·05	0·03
CaO	0·19	0·54	0·01	0·09	0·12	0·16	6·00	1·70
Cr_2O_3	0·01	0·00	0·04	0·00	0·02	0·05	0·00	0·11
Total	98·80	98·48	99·12	98·89	98·50	99·19	99·12	99·38
FeO	43·57	41·64	42·81	40·42	43·80	42·85	30·98	35·71
Fe_2O_3	2·42	3·70	4·51	5·42	2·66	3·45	9·72	6·93
Total	99·04	98·85	99·57	99·44	98·77	99·53	100·09	100·07
% R_2O_3	2·33	3·63	4·39	5·74	2·61	3·46	9·44	6·94
T (°C)	680	912	790	900				
Log(fO_2)	−19·5	−13·1	−15·5	−13·0				

Temperature and log(fO_2) according to Buddington & Lindsley (1964) for homogeneous magnetite–ilmenite pairs. FeO, Fe_2O_3, ulvöspinel (Ulv.) and R_2O_3 calculated according to Carmichael (1967).

(Table 4). The corresponding log(fO_2) values range from −19·5 to −13·0 (Buddington & Lindsley, 1964), corresponding to conditions intermediate between fayalite–magnetite–quartz (FMQ) and wüstite–magnetite (WM) buffers (Fig. 5).

The scarce HTi tholeiitic dykes (D2) have ophitic textures. Labradoritic plagioclase is often altered to clay minerals and sericite and sometimes albitized (Ab up to 98%). Pyroxenes are augites (Wo 40–38) with high TiO_2 content (1·2–1·4 wt %; Table 2) and

Table 5: Major and trace element compositions of tholeiitic (D1, D1a, D2) and calc-alkaline (D3, D4) dykes from the Azul and Tandil regions

Sample:	A1	A2	A4	A5	A8	A9	A10	A16	A25
Locality:	AZUL	AZUL	AZUL	AZUL	AZUL	AZUL	AZUL	AZUL	AZUL
Direction:	N–S	N–S	N30°W	N40°W	N40°W	N40°W	N40°W	N80°E	N35°W
Rock:	ThB	ThB	ThB	ThB	ThB	ThB	ThB	ThB	ThB
Group:	D1	D1	D1	D1	D1	D1	D1	D1	D1
SiO_2 (wt %)	50·55	50·20	50·76	50·72	50·86	50·42	50·03	50·48	51·34
TiO_2	1·26	1·29	1·16	0·99	1·19	1·36	1·21	0·92	0·87
Al_2O_3	14·22	14·85	14·07	14·66	14·17	15·17	14·72	17·73	14·69
FeO_{tot}	12·11	12·11	11·61	10·72	11·91	12·31	12·42	10·21	10·56
MnO	0·20	0·19	0·19	0·18	0·19	0·19	0·20	0·16	0·19
MgO	7·73	7·00	8·00	8·02	7·40	6·71	8·49	6·47	8·16
CaO	10·77	11·55	11·46	12·24	11·39	9·46	9·09	10·56	11·21
Na_2O	2·15	2·27	2·16	2·17	2·27	2·30	2·15	2·40	2·06
K_2O	0·87	0·42	0·46	0·19	0·48	1·93	1·56	0·97	0·83
P_2O_5	0·14	0·12	0·13	0·11	0·14	0·15	0·13	0·10	0·09
mg-no.	56·35	53·89	58·22	60·20	55·68	52·43	58·02	56·17	60·98
LOI (wt %)	2·02	1·40	1·84	1·47	2·36	2·63	3·55	1·36	2·41
FeO (wt %)	9·95	10·15	9·48	9·00	9·27	9·20	9·76	9·14	8·82
Fe_2O_3 (wt %)	2·40	2·18	2·37	1·91	2·93	3·46	2·96	1·19	1·93
Cr (ppm)	328	292	345	356	336	196	272	239	157
Ni	137	144	140	147	127	115	131	134	110
Rb	51	17	18	7	20	71	62	108	96
Ba	87	99	61	31	47	165	274	136	65
Sr	176	154	160·00	138	164	166	263	171	201
Nb	4	6	6	5	6	6	9	2	3
Zr	87	77	73	74	91	89	85	89	62
Y	27	26	20	22	30	30	28	26	20
La	6	*3·62**	3	*3·60**	*4·41**	6	5	*7·33**	*2·77**
Ce	19	*9·35*	21	*9·56*	*11·82*	14	15	*15·41*	*7·28*
Pr		*1·30*		*1·33*	*1·78*			*1·95*	*1·05*
Nd	11	*7·29*	10	*7·09*	*9·57*	14	10	*9·08*	*5·22*
Sm		*2·57*		*2·31*	*2·98*			*2·46*	*1·78*
Eu		*1·00*		*0·80*	*0·98*			*0·87*	*0·65*
Gd		*3·35*		*2·99*	*3·37*			*2·96*	*2·01*
Tb		*0·49*		*0·43*	*0·53*			*0·43*	*0·33*
Dy		*3·16*		*2·95*	*3·69*			*2·69*	*2·26*
Ho		*0·71*		*0·70*	*0·88*			*0·64*	*0·49*
Er		*1·86*		*1·75*	*2·22*			*1·73*	*1·25*
Tm		*0·27*		*0·26*	*0·32*			*0·27*	*0·18*
Yb		*1·96*		*1·80*	*2·14*			*1·89*	*1·31*
Lu		*0·28*		*0·27*	*0·30*			*0·27*	*0·20*
Q (CIPW)	0·00	0·00	0·00	0·00	0·00	0·00	0·00	0·00	0·00
Ol/Hy (CIPW)	0·20	0·15	0·10	0·10	0·07	0·76	0·71	0·34	0·09

Sample:	A30	A32	A33	A34	A35	MT65	MT66	MT55	Mean	SD
Locality:	TANDIL	TANDIL	TANDIL	TANDIL	TANDIL	TANDIL	TANDIL	TANDIL	$n = 34$	(1σ)
Direction:	N30°W	E–W	E–W	N30°W	N30°W	N10°W	N10°W	N30°W		
Rock:	BTrand	ThB	ThB	ThB	ThB	ThB	ThB	ThB		
Group:	D1	D1	D1	D1	D1	D1	D1	D1	D1	D1
SiO_2 (wt %)	52·46	48·72	50·86	50·36	50·67	50·62	50·69	50·00	50·61	0·59
TiO_2	1·55	0·91	1·23	1·31	1·28	1·43	1·24	1·66	1·19	0·18
Al_2O_3	15·55	15·65	14·28	14·48	15·41	12·99	14·34	16·17	14·89	1·09
FeO_{tot}	13·56	12·46	12·78	13·29	12·29	13·24	11·89	13·87	11·93	1·01
MnO	0·15	0·20	0·20	0·21	0·20	0·22	0·21	0·20	0·19	0·02
MgO	3·82	8·44	7·57	6·93	6·32	7·46	7·59	4·63	7·28	0·89
CaO	7·28	9·66	9·64	10·01	10·03	10·87	11·56	9·45	10·49	1·06
Na_2O	4·75	2·30	2·16	2·15	2·35	2·33	2·00	2·60	2·31	0·48
K_2O	0·64	1·22	1·14	1·14	1·33	0·64	0·33	1·19	0·96	0·42
P_2O_5	0·24	0·44	0·14	0·12	0·12	0·14	0·10	0·18	0·14	0·06
mg-no.	36·29	57·80	54·50	51·32	50·98	53·26	56·35	40·30	55·11	4·43
LOI (wt %)	3·22	3·42	2·61	2·02	2·88	3·50	2·33	3·11	2·36	0·65
FeO (wt %)	9·44	10·44	9·58	10·68	9·85	7·49	4·73	10·15	9·40	1·24
Fe_2O_3 (wt %)	4·58	2·24	3·56	2·90	2·71	1·96	1·06	4·13	2·44	0·86
Cr (ppm)	14	144	144	139	94	165	171	71	220	85
Ni	29	76	129	122	85	101	100	57	117	26
Rb	29	64	29	48	48	30	15	35	62	47
Ba	63	318	90	233	110	127	30	64	130	70
Sr	326	302	173	156	156	205	189	238	198	56
Nb	14	10	6	9	4	4	3	7	6	3
Zr	142	96	78	96	76	97	59	96	85	15
Y	44	27	26	26	24	22	15	18	26	5
La	11	12	*3·51**	*5·26**	4	5	4	3	6	3
Ce	30	33	*9·63*	*13·19*	18	13	8	13	18	5
Pr			*1·53*	*1·90*						
Nd	19	18	*8·02*	*9·17*	9	10	7	15	11	3
Sm			*2·54*	*2·96*						
Eu			*0·94*	*0·97*						
Gd			*2·93*	*3·47*						
Tb			*0·47*	*0·55*						
Dy			*3·30*	*3·76*						
Ho			*0·75*	*0·84*						
Er			*2·00*	*2·23*						
Tm			*0·28*	*0·33*						
Yb			*1·92*	*2·26*						
Lu			*0·29*	*0·35*						
Q (CIPW)	0·00	0·00	0·00	0·00	0·00	0·00	0·43	0·00		
Ol/Hy (CIPW)	1·13	1·63	0·13	0·19	0·28	0·16	0·00	0·18		

Table 5: continued

Sample:	A19	A20	A21	A22	Mean	SD	A38	A39	A53
Locality:	AZUL	AZUL	AZUL	AZUL	$n = 4$	(1σ)	TANDIL	TANDIL	TANDIL
Direction:	N30°W	N30°W	N30°W	N30°W			E–W	E–W	E–W
Rock:	BAnd	BAnd	BAnd	BAnd			Trb	ThB	ThB
Group:	D1a	D1a	D1a	D1a	D1a	D1a	D2	D2	D2
SiO_2 (wt %)	53·69	53·62	53·72	53·68	53·68	0·04	47·99	48·11	49·58
TiO_2	1·20	1·20	1·22	1·21	1·21	0·01	3·74	3·61	2·14
Al_2O_3	15·34	15·58	15·27	15·75	15·49	0·22	14·16	13·99	13·06
FeO_{tot}	11·52	11·45	11·52	11·49	11·50	0·03	14·76	15·83	15·25
MnO	0·18	0·18	0·18	0·18	0·18	0·00	0·23	0·22	0·23
MgO	4·71	4·98	4·71	4·47	4·72	0·21	5·42	3·87	6·72
CaO	8·86	7·97	8·24	7·97	8·26	0·42	6·94	9·17	8·71
Na_2O	2·89	2·95	2·89	2·95	2·92	0·03	2·71	2·05	2·25
K_2O	1·26	1·72	1·91	1·93	1·71	0·31	2·58	1·63	0·90
P_2O_5	0·35	0·35	0·34	0·37	0·35	0·01	1·47	1·52	1·16
mg-no.	45·26	46·79	45·26	44·03	45·34	1·13	42·61	33·08	47·12
LOI (wt %)	2·02	2·54	2·62	2·46	2·41	0·27	3·61	3·64	3·11
FeO (wt %)	10·85	10·20	10·08	10·79	10·48	0·40	11·22	12·80	12·24
Fe_2O_3 (wt %)	0·74	1·39	1·60	0·78	1·13	0·43	3·93	3·37	3·34
Cr (ppm)	109	104	110	102	106·25	3·86	54	58	149
Ni	22	18	21	19	20·00	1·83	33	24	74
Rb	36	55	63	58	53·00	11·80	81	47	34
Ba	681	776	750	865	768·00	76·08	932	976	477
Sr	298	335	353	340	331·50	23·59	309	488	367
Nb	15	14	13	12	13·50	1·29	47	51	15
Zr	192	190	195	188	191·25	2·99	390	415	205
Y	39	36	39	39	38·25	1·50	62	66	37
La	*30·60**	37	41	41	37·40	4·91	*43·66**	48	49
Ce	*62·00*	72	75	72	70·25	5·68	*87·12*	96	91
Pr	*6·93*						*9·82*		
Nd	*26·95*	38	39	36	34·99	5·50	*44·49*	58	55
Sm	*5·37*						*9·87*		
Eu	*1·61*						*3·55*		
Gd	*5·19*						*10·45*		
Tb	*0·73*						*1·41*		
Dy	*4·80*						*7·73*		
Ho	*1·06*						*1·66*		
Er	*2·80*						*3·95*		
Tm	*0·43*						*0·61*		
Lu	*0·46*						*0·68*		
Q (CIPW)	3·43	2·06	2·09	2·12			0·00	2·92	1·32
Ol/Hy (CIPW)	0·00	0·00	0·00	0·00			0·44	0·00	0·00

Sample:	MT67	MT68	MT69	MT70	Mean	SD	A40	A41	A49	A52
Locality:	TANDIL	TANDIL	TANDIL	TANDIL	$n = 7$	(1σ)	TANDIL	TANDIL	TANDIL	TANDIL
Direction:	N15°W	N15°W	N70°W	N70°E			N80°E	N80°E	E–W	N40°W
Rock:	ThB	ThB	ThB	ThB			BAnd	BAnd	BAnd	BAnd
Group:	D2	D2	D2	D2	D2	D2	D3	D3	D3	D3
SiO_2 (wt %)	48·28	49·04	50·24	48·66	48·84	0·83	56·55	58·20	56·04	56·03
TiO_2	1·90	1·71	2·45	1·96	2·50	0·83	0·77	0·80	0·74	0·43
Al_2O_3	14·42	14·02	14·02	14·16	13·98	0·43	13·59	14·26	14·12	15·26
FeO_{tot}	14·62	15·31	14·31	14·95	15·00	0·50	9·39	8·45	9·53	8·67
MnO	0·22	0·22	0·23	0·22	0·22	0·01	0·19	0·17	0·19	0·17
MgO	6·88	6·55	5·57	6·43	5·92	1·06	6·97	5·40	6·88	7·22
CaO	9·33	8·97	8·93	8·82	8·70	0·80	8·36	7·12	8·28	8·36
Na_2O	2·37	2·34	2·57	2·69	2·43	0·24	2·86	3·10	2·23	2·43
K_2O	0·95	0·95	0·93	1·04	1·28	0·63	0·93	2·21	1·61	1·31
P_2O_5	0·96	0·80	0·67	0·98	1·08	0·32	0·39	0·29	0·38	0·12
mg-no.	48·76	46·38	44·04	46·52	44·07	5·25	60·02	56·37	59·35	62·74
LOI (wt %)	2·44	3·13	1·96	3·29	3·03	0·62	3·03	2·52	3·01	3·29
FeO (wt %)	9·48	10·88	9·56	12·06	11·18	1·30	7·10	6·44	7·11	7·31
Fe_2O_3 (wt %)	3·21	2·62	2·59	2·84	3·13	0·48	2·54	2·23	2·69	1·51
Cr (ppm)	92	117	132	78	97	37	241	114	194	60
Ni	104	84	77	83	68	29	19	14	20	21
Rb	46	46	51	41	49	15	49	93	59	48
Ba	493	505	402	529	616	234	353	754	493	354
Sr	448	392	388	422	402	58	564	666	595	456
Nb	17	16	15	14	25	16	9	10	9	5
Zr	167	187	230	183	254	104	119	126	117	74
Y	24	24	24	25	37	19	23	21	21	14
La	30	28	32	30	39	11	30	*26·32**	23	12
Ce	72	57	78	63	80	17	63	*56·85*	55	33
Pr								*6·53*		
Nd	37	37	46	40	48	10	31	*28·01*	30	14
Sm								*6·53*		
Eu								*6·53*		
Gd								*6·53*		
Tb								*6·53*		
Dy								*6·53*		
Ho								*6·53*		
Er								*6·53*		
Tm								*6·53*		
Yb								*6·53*		
Lu								*6·53*		
Q (CIPW)	0·00	0·00	1·44	0·00			6·88	7·10	7·02	5·74
Ol/Hy (CIPW)	0·32	0·14	0·00	0·39			0·00	0·00	0·00	0·00

Table 5: continued

Sample:	A54	T12	Mean	SD	A45	A46	A47	A48	A51
Locality:	TANDIL	TANDIL	$n = 9$	(1σ)	TANDIL	TANDIL	TANDIL	TANDIL	TANDIL
Direction:	E–W	E–W			N80°E	E–W	E–W	E–W	E–W
Rock:	And	And			Rhy	Rhy	Rhy	Rhy	Rhy
Group:	D3	D3	D3	D3	D4	D4	D4	D4	D4
SiO_2 (wt %)	59·77	58·03	57·22	1·25	74·44	73·84	75·01	73·82	76·21
TiO_2	0·78	0·77	0·72	0·11	0·14	0·19	0·12	0·15	0·11
Al_2O_3	14·57	13·33	14·12	0·72	13·23	13·77	13·06	13·42	12·72
FeO_{tot}	8·52	8·58	8·91	0·40	2·28	1·97	1·96	2·38	1·88
MnO	0·16	0·18	0·18	0·01	0·05	0·04	0·06	0·06	0·03
MgO	3·68	7	6·21	1·25	0·11	0·21	0·01	0·03	0·17
CaO	6·28	8·05	7·88	0·79	1·17	1·33	0·98	1·31	1·30
Na_2O	3·75	2·49	2·78	0·49	4·25	3·91	4·19	4·52	3·84
K_2O	2·17	1·28	1·67	0·45	4·32	4·70	4·61	4·30	3·72
P_2O_5	0·32	0·29	0·32	0·08	0·01	0·04	0·01	0·01	0·02
mg-no.	46·62	61·77	57·72	5·30	8·89	17·73	1·02	2·48	15·46
LOI (wt %)	1·65	2·66	2·73	0·56	0·76	0·70	0·65	0·57	0·62
FeO (wt %)	6·80	6·31	6·88	0·39	2·18	1·75	1·57	2·19	1·62
Fe_2O_3 (wt %)	1·91	1·64	1·85	0·56	0·11	0·24	0·43	0·21	0·29
Cr (ppm)	45	361	186	119	1	3	3	1	2
Ni	12	35	20	8	3	2	1	1	5
Rb	154	63	82	35	145	178	148	139	141
Ba	517	474	520	130	1219	1185	1355	1326	802
Sr	375	570	552	88	181	261	135	182	178
Nb	9	5	8	2	12	13	12	12	11
Zr	135	132	113	20	273	213	227	233	169
Y	29	22	22	4	33	22	30	29	26
La	*24·02**	30	26	6	57	*56·62**	*53·80**	55	56
Ce	*54·46*	63	58	12	108	*105·10*	*106·40*	101	107
Pr	*6·43*					*10·35*	*11·36*		
Nd	*25·83*	32	30	7	49	*36·86*	*42·04*	48	49
Sm	*4·85*					*6·05*	*6·94*		
Eu	*1·02*					*1·11*	*1·21*		
Gd	*3·86*					*4·53*	*5·30*		
Tb	*0·53*					*0·55*	*0·74*		
Dy	*3·18*					*2·74*	*4·34*		
Ho	*0·66*					*0·50*	*0·78*		
Er	*1·50*					*1·36*	*1·96*		
Tm	*0·24*					*0·22*	*0·29*		
Yb	*1·61*					*1·47*	*2·11*		
Lu	*0·26*					*0·22*	*0·33*		
Q (CIPW)	8·91	9·90			29·36	28·85	29·94	27·27	35·41
Ol/Hy (CIPW)	0·00	0·00			0·00	0·00	0·00	0·00	0·00

Sample:	A36	BR1	BR2	mean	SD	A50	A44	LP3	SL1
Locality:	TANDIL	TANDIL	TANDIL	$n = 8$	(1σ)	TANDIL	TANDIL	TANDIL	TANDIL
Direction:	E–W	E–W	E–W						
Rock:	Dacite	Rhy	Rhy			Granite	Diorite	Diorite	Gabbro
Group:	D4	D4	D4	D4	D4				
SiO_2 (wt %)	66·41	72·98	74·06	73·35	2·96	69·71	65·82	54·81	49·45
TiO_2	0·50	0·20	0·14	0·19	0·13	0·34	0·55	0·94	0·44
Al_2O_3	14·26	14·23	13·66	13·54	0·54	16·08	15·00	19·69	14·59
FeO_{tot}	5·56	1·87	2·16	2·51	1·25	2·64	5·29	7·44	8·42
MnO	0·11	0·04	0·05	0·06	0·02	0·03	0·11	0·13	0·16
MgO	3·01	0·32	0·04	0·49	1·02	1·09	2·48	3·05	11·22
CaO	3·73	1·50	1·22	1·57	0·89	3·79	4·66	8·99	13·71
Na_2O	3·26	3·89	4·95	4·10	0·50	4·73	4·28	3·05	1·21
K_2O	2·99	4·82	3·63	4·14	0·63	1·48	1·57	1·34	0·50
P_2O_5	0·17	0·06	0·02	0·04	0·05	0·11	0·24	0·45	0·19
mg-no.	52·26	25·71	3·61	15·90	17·00	45·50	48·67	45·32	72·93
LOI (wt %)	2·52	3·24	3·01	1·51	1·19	0·86	1·66	n.m.	n.m.
FeO (wt %)	4·20	12·51	12·37	4·80	4·79	2·64	4·68	n.m.	n.m.
Fe_2O_3 (wt %)	1·51	3·11	2·16	1·01	1·13	0·00	0·68	n.m.	n.m.
Cr (ppm)	66	4	2	10	23	1	19	54	327
Ni	10	0	0	3	3	2	10	7	40
Rb	112	201	123	148	29	37	80	39	13
Ba	912	1220	1184	1150	194	913	567	432	301
Sr	519	326	242	253	123	1021	751	862	548
Nb	10	9	10	11	1	3	11	11	7
Zr	174	201	268	220	39	80	108	62	51
Y	26	15	35	27	6	3	16	12	8
La	*38·70**	*59·36**	49	54	6	14	16	15	19
Ce	*79·44*	*117·20*	98	101	12	28	35	46	47
Pr	*8·41*	*11·94*							
Nd	*30·69*	*42·33*	41	45	6	9	15	19	28
Sm	*5·42*	*5·96*							
Eu	*1·15*	*1·13*							
Gd	*4·27*	*3·38*							
Tb	*0·58*	*0·45*							
Dy	*3·40*	*2·23*							
Ho	*0·71*	*0·43*							
Er	*1·70*	*1·11*							
Tm	*0·25*	*0·15*							
Yb	*1·80*	*1·01*							
Lu	*0·28*	*0·15*							
Q (CIPW)	20·88	27·21	27·67						
Ol/Hy (CIPW)	0·00	0·00	0·00						

*REE values in italics were measured by ICP-AES.
ThB, tholeiitic basalt; BTrand, basaltic trachyandesite; BAnd, basaltic andesite; Trb, trachybasalt; And, andesite; Rhy, rhyolite. FeO_{tot}, total Fe as FeO; *mg*-number, 100 × at. Mg/(Mg + Fe^{2+}) for $Fe_2O_3/FeO = 0·15$. Q, Ol and Hy are CIPW normative quartz, olivine and hypersthene. n.m., not measured.

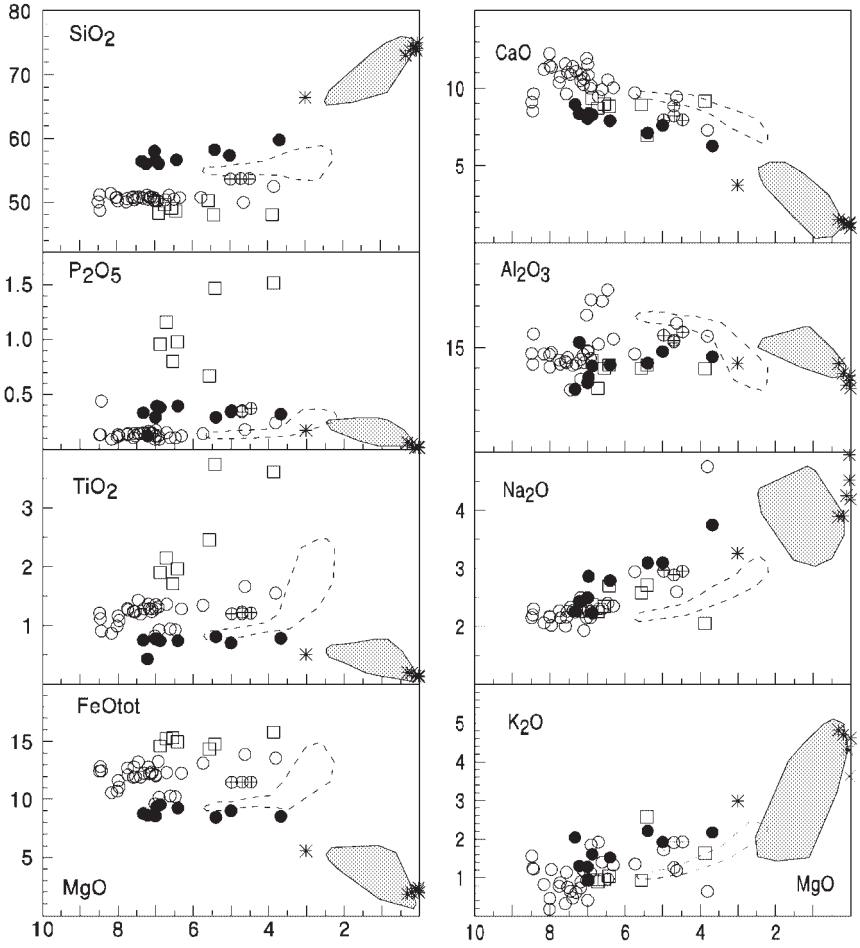

Fig. 6. MgO (wt %) vs major elements (wt %) for Azul and Tandil dyke swarms. Symbols as in Fig. 4; also, crossed circles, D1a tholeiitic dykes; *, rhyolite (D4) dykes. Fields outlined with continuous line, dyke country rocks; fields outlined with dashed line, 1·7 Ga Florida (Uruguay) tholeiitic dyke swarms (Bossi *et al.*, 1993).

pigeonite. Pyroxenes may be replaced by hornblende, actinolite–tremolite and chlorite. Ilmenite (Table 4), magnetite, rutile and pyrite (Echeveste & Fernandez, 1994), and apatite are abundant in the groundmass.

The basic–intermediate calc-alkaline dykes (D3) have porphyritic to intergranular textures. The porphyritic dykes have phenocrysts of plagioclase ($An_{55–34}$, Table 1), often altered to sericite and clay minerals, and salitic–augitic pyroxenes (Table 2), almost completely replaced by amphiboles and opaque minerals. The holocrystalline matrix is composed of microphenocrysts of altered plagioclase, epidote, biotite–chlorite, opaques (ilmenite, Table 4; pyrrotite, Echeveste & Fernandez, 1994), altered alkali-feldspar and quartz. The dykes with intergranular texture have plagioclase and augite completely replaced by secondary minerals. Quartz–feldspar intergrowths are present in the groundmass.

The dacitic and rhyolitic dykes (D4) have a porphyritic texture, phenocrysts of altered plagioclase, alkali-feldspar and augite being replaced by amphibole–chlorite aggregates. The same minerals are found in the holomicrocrystalline matrix. Secondary zeolites or quartz and K-feldspars may fill vesicles or fractures.

GEOCHEMISTRY

Major and trace elements were determined using a PW 1404 XRF spectrometer, following the procedures of Philips (1994) for the correction of matrix effects. Results are accurate to within 2–3% for major elements and better than 7–10% for trace elements. Ferrous iron was determined by redox titration; loss on ignition (LOI) was determined at 1100°C (12 h) and corrected for Fe^{2+} oxidation. Rare earth elements (REE) were determined by inductively coupled plasma-atomic emission spectrometry (ICP-AES) at the Centre de Recherches Petrographiques et Géochimiques, CNRS,

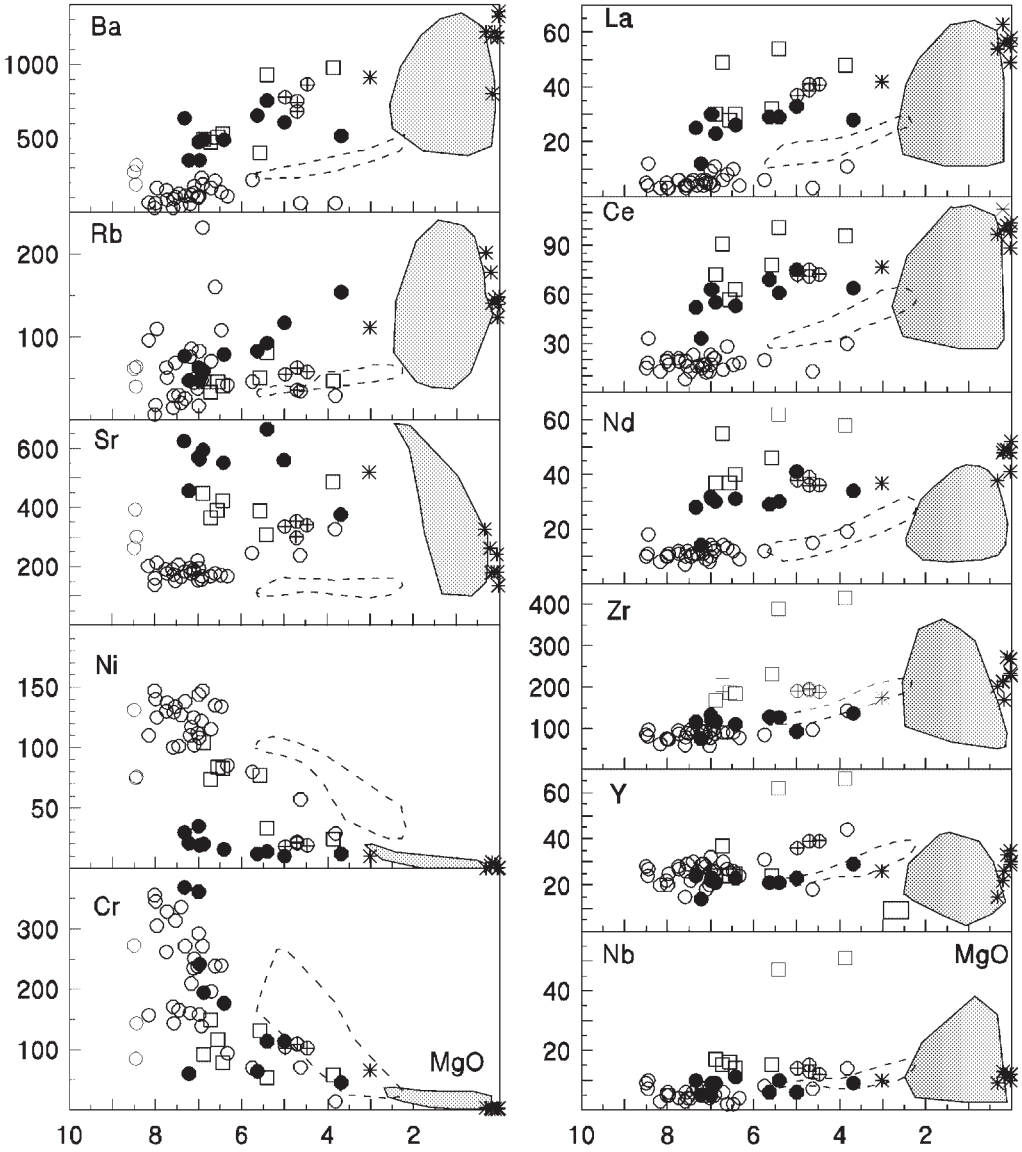

Fig. 7. MgO (wt %) vs trace elements (ppm) for Azul and Tandil dyke swarms. Symbols as in Figs 4 and 6.

Vandoeuvre (France) (Govindaraju & Mevelle, 1987).

Low-TiO_2 (LTi) tholeiites (Table 5) have SiO_2 and MgO contents ranging from 48·7 to 53·7 wt % (mean 51·0 ± 1·2 wt %) and 8·8 to 3·8 wt %, respectively, and *mg*-number values from 61 to 36. As shown in the variation diagrams (Figs 6 and 7), with respect to MgO, the trend of SiO_2 is rather flat, like that of P_2O_5 (0·12 ± 0·03 wt %), TiO_2 (1·34 ± 0·13 wt %) and FeO_{tot} (12·6 ± 1·0 wt %). The D1 dykes plotting in the basalt field have low contents of incompatible elements (IE), whereas those with basaltic andesite composition (D1a), for similar MgO, have higher IE (e.g. La, Ce, Nd, Zr; Fig. 7). D1a dykes also have La/Y (~1·0) and Zr/Y (~5·0) that are clearly higher (Fig. 8) than those of the D1 dykes (~0·3 and 3–4, respectively), excluding the possibility that they derived from D1 basalt dykes through simple fractional crystallization. It should be noted that the D1 tholeiites have REE patterns (Fig. 9) similar to the E-MORB of Sun & McDonough (1989), with mean chondrite-normalized $(La/Yb)_{CN}$ of 1·55 ± 0·48, whereas the D1a-type tholeiite is more fractionated, i.e. $(La/Yb)_{CN}$ = 6·83. Considerable differences between D1 and D1a tholeiites are also apparent, excluding mobile elements such as Rb, Ba and K, in the multi-elemental diagram relative to the Primitive Mantle (PM) of Sun & McDonough (1989; Fig. 9), in which the $(La/Nb)_{PM}$ and $(Zr/Ti)_{PM}$ ratios of D1 dykes are lower than those

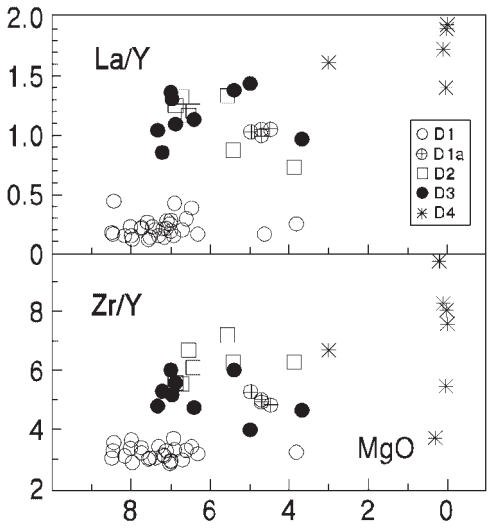

Fig. 8. MgO (wt %) vs Zr/Y and La/Y ratios for Azul and Tandil dyke swarms.

of IE-enriched D1a dykes (1·06 ± 0·78 vs 2·92 ± 0·63, and 1·31 ± 0·36 vs 3·07 ± 0·04, respectively).

High-TiO_2 (HTi) tholeiites have MgO ranging from 6·9 to 3·9 wt % (*mg*-number 49–33) and relatively low SiO_2 contents (48·8 ± 0·8 wt %). They are characterized by high concentrations of TiO_2 (1·71–3·74, mean 2·50 ± 0·83 wt %), P_2O_5 (0·67–1·52 wt %), REE, Zr (254 ± 104 ppm) and Nb (25 ± 16 ppm). The REE pattern (A38) of a D2 dyke parallels that of the D1a basaltic andesite (LTi), and is similarly characterized by high $(La/Yb)_{CN}$ (6·72). In the multi-elemental diagram, the HTi dykes have enriched IE patterns with respect to LTi dykes, being characterized by positive P and negative Sr and Ti (Zr/Ti_{PM} = 1·93 ± 0·19) spikes. It should be noted that $(La/Nb)_{PM}$ ranges from 1·0 to 3·4 (mean = 1·92 ± 0·83).

The calc-alkaline basaltic andesites and andesites have MgO and SiO_2 ranging from 7·0 to 3·7 wt % (*mg*-number 60–47) and 56·0 to 59·8 wt %, respectively. These dykes (D3), relative to the D1 tholeiites, have lower mean TiO_2 (0·72 vs 1·20 wt %) and FeO_{tot} (8·9

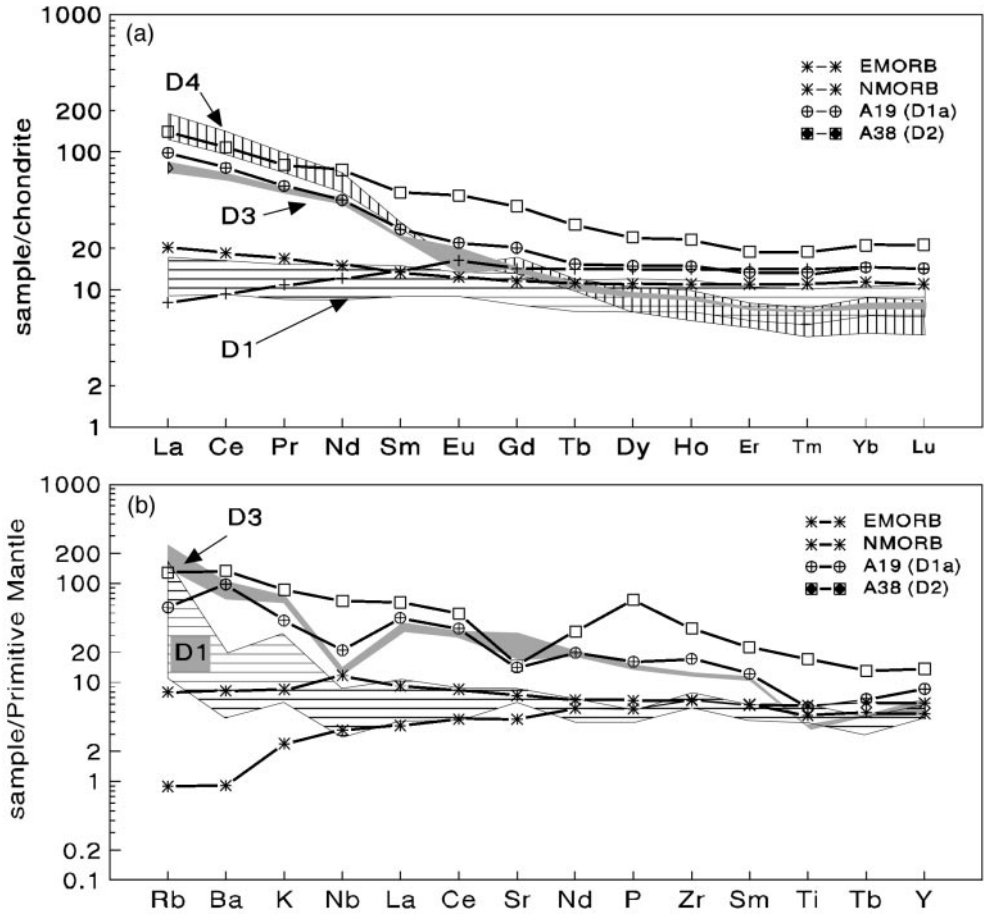

Fig. 9. (a) Chondrite-normalized (Boynton, 1984) REE abundance patterns of tholeiitic (D1, D1a, D2) and calc-alkaline (D3, D4) dyke swarms from Azul and Tandil regions. (b) Incompatible element patterns, normalized to Primitive Mantle of Sun & McDonough (1989), for tholeiitic and calc-alkaline dyke swarms from the Azul and Tandil regions.

Table 6: $^{87}Sr/^{86}Sr$ isotopic compositions (2σSD in parentheses) of tholeiitic (D1, D2), calc-alkaline (D3, D4) dykes and country rocks from the Azul and Tandil regions

Sample	Rb (ppm)	Sr (ppm)	$^{87}Sr/^{86}Sr$	Sr_i	εSr
D1 Group (1588 Ma)					
A1 (ThB)	40·89	166·93	0·72416(20)	0·70797	76
A2 (ThB)	16·50	149·62	0·71025(16)	0·70297	5
A4 (ThB)	16·85	166·20	0·71370(14)	0·70701	63
A5 (ThB)	5·74	134·16	0·70717(18)	0·70435	24
A8 (ThB)	16·70	157·18	0·71314(24)	0·70613	50
A33 (ThB)	29·79	195·91	0·71508(18)	0·70504	34
A35 (ThB)	42·09	171·38	0·72639(20)	0·71016	107
MT65 (ThB)	29·71	192·44	0·71540(14)	0·70521	35
D2 Group (1588 Ma)					
A38 (Trb)	62·48	237·91	0·72187(18)	0·70452	27
A39 (ThB)	37·53	453·13	0·71218(18)	0·70671	58
A53 (ThB)	29·84	330·84	0·70895(18)	0·70300	5
MT67 (ThB)	39·26	404·26	0·71705(18)	0·71064	114
MT68 (ThB)	38·68	370·56	0·71785(16)	0·71096	118
MT69 (ThB)	45·87	360·57	0·71228(18)	0·70388	18
MT70 (ThB)	33·21	393·17	0·71425(34)	0·70867	86
D3 group (2020 Ma)					
A40 (BAnd)	42·00	577·84	0·70987(14)	0·70375	23
A41 (BAnd)	58·79	663·02	0·71250(11)	0·70503	41
A49 (BAnd)	51·96	577·19	0·71125(11)	0·70367	22
A52 (BAnd)	43·76	507·00	0·71046(16)	0·70319	15
A54 (And)	147·76	378·90	0·73667(16)	0·70373	23
D4 group (2020 Ma)					
A47 (Rhy)	142·52	142·55	0·78779(16)	0·70293	12
BR2 (Rhy)	117·50	251·61	0·74389(18)	0·70440	32
Country rocks (2150 Ma)					
A50 (granite)	31·83	1057·71	0·70524(24)	0·70254	8
SL2 (gabbro)	13·37	551·99	0·70457(12)	0·70240	6
LP3 (diorite)	37·18	899·70	0·70693(18)	0·70322	18
A44 (diorite)	64·54	671·64	0·71270(16)	0·70476	30

Rb and Sr measured by isotope dilution. Abbreviations as in Table 5.

vs 11·9 wt %) and higher P_2O_5 (0·32 vs 0·14 wt %), Sr (552 vs 199 ppm), REE (e.g. La 26 vs 6 ppm; Nd 30 vs 11 ppm) and Zr (113 vs 86). The REE patterns of D3 dykes (Fig. 9) are different from those of tholeiitic D1 and D2 dykes, and are characterized by the highest $(La/Yb)_{CN}$ values, i.e. 10–12. In the multi-elemental diagram (Fig. 9), D3 dykes are distinct from the others by having pronounced negative spikes of Nb (La/Nb_{PM} = 3·39 ± 1·43) and Ti (Zr/Ti_{PM} = 3·18 ± 0·15).

The silicic dykes (SiO_2 65–75 wt %) have the highest IE contents and are characterized by very high $(La/Yb)_{CN}$ (15–40) and a significant Eu negative anomaly (Eu/Eu* = 0·61–0·76).

ISOTOPE GEOCHEMISTRY

Sr and Nd isotope analyses of selected samples were performed at the 'Centro de Pesquisas Geocronológicas'

Table 7: $^{143}Nd/^{144}Nd$ isotopic compositions (2σSD in parentheses) of tholeiitic (D1, D2) and calc-alkaline (D3, D4) dykes from the Azul and Tandil regions

Sample	Sm (ppm)	Nd (ppm)	$^{143}Nd/^{144}Nd$	Nd_i	εNd
D1 Group (1588 Ma)					
A4 (ThB)	1·900	7·635	0·512778(39)	0·511206	12·18
A5 (ThB)	2·280	6·926	0·512893(41)	0·510814	4·49
A16 (ThB)	2·571	9·633	0·512250(20)	0·510564	−0·39
D2 Group (1588 Ma)					
A38 (Trb)	10·433	48·003	0·511895(20)	0·510518	−1·30
MT70 (ThB)	7·285	38·939	0·511394(37)	0·510242	−6·71
D3 Group (2020 Ma)					
A40 (BAnd)	−4·667	25·056	0·511375(38)	0·509878	−2·84
A41 (BAnd)	4·925	26·675	0·511323(40)	0·509839	−3·59
A54 (And)	5·179	26·699	0·511392(10)	0·509832	−3·73
D4 Group (2020 Ma)					
A48 (Rhy)	4·260	22·531	0·511372(40)	0·509852	−3·34
A51 (Rhy)	7·063	40·709	0·511190(10)	0·509795	−4·45

Sm and Nd measured by isotope dilution. Abbreviations as in Table 5.

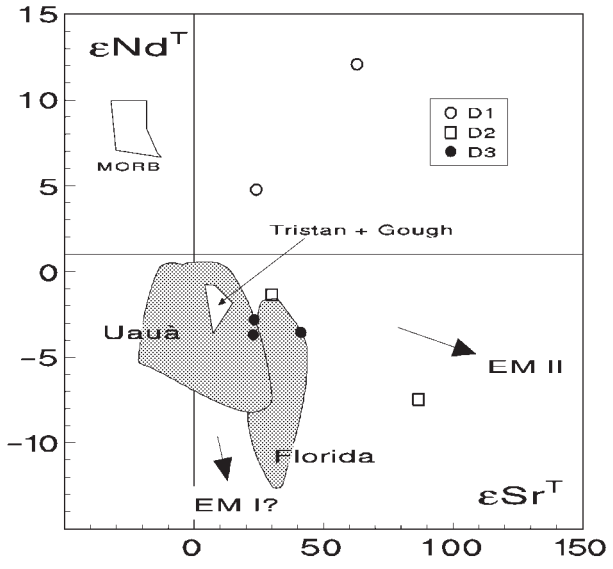

Fig. 10. εSr^T vs εNd^T diagram for tholeiitic and calc-alkaline dyke swarms of the Azul and Tandil regions. Fields of MORB, Uauà (2·2–2·0 Ga, São Francisco craton, Brazil; Bellieni *et al.*, 1995) and Florida (1·7 Ga, Rio de La Plata craton, Uruguay; Mazzucchelli *et al.*, 1995; Teixeira *et al.*, 1999) are shown for comparison. EMI and EMII after Hart & Zindler (1989).

of São Paulo, following the procedure of Ludwig (1985). Rb, Sr, Sm and Nd concentrations were measured by isotopic dilution. The average $^{87}Sr/^{86}Sr$ for NBS-987 and $^{143}Nd/^{144}Nd$ for La Jolla standards were 0·710254(22) and 0·511857(46), respectively, with 2σ standard deviations reported in parentheses.

The initial $^{87}Sr/^{86}Sr$ (Sr_i) and $^{143}Nd/^{144}Nd$ (Nd_i) were calculated to 1588 Ma (baddeleyite U–Pb age: Teixeira *et al.*, in preparation) for D1 and D2 dykes, 2020 Ma (biotite $^{40}Ar/^{39}Ar$ age: Teixeira *et al.*, in preparation) for D3 and D4 dykes, and 2150 Ma for the country rocks.

The studied dykes have Sr_i ratios (Table 6) higher than those of Bulk Earth (BE): tholeiitic dykes: 0·7030–0·7102 for D1 (εSr 5–107), 0·7030–0·7110 for D2 (εSr 6–118); calc-alkaline dykes: 0·7032–0·7050 for D3 (εSr 15–41) and 0·7029–0·7044 for D4 (εSr 12–32). The gabbroic to granitic country rocks have Sr_i ranging from 0·7025 to 0·7048 (εSr 8–30), as reported by Varela *et al.* (1988) for the 'old granitoids'. The 'young granitoids' of the basement have $Sr_{i(1750\,Ma)}$ in the range 0·7181–0·7303 (εSr 221–395; Varela *et al.*, 1985, 1988; Dalla Salda *et al.*, 1992).

The initial $^{143}Nd/^{144}Nd$ (Table 7) of the LTi tholeiitic dykes (D1) ranges from 0·51056 to 0·51121 and is slightly lower to higher relative to BE (εNd −0·4 to 12·2). In comparison, the HTi tholeiitic dykes (D2) are moderately (Nd_i = 0·51052, εNd = −1·3) to much (Nd_i = 0·51024, εNd = −6·71) lower than BE. D3 and D4 andesitic and rhyolitic dykes have similar Nd_i (0·50980–0·50988) and are moderately lower than BE (εNd = −2·8 to −4·5).

Table 8: Mineral–liquid partition coefficients used for fractional crystallization modelling (see text for explanation)

	Ol/liq	Cpx/liq	Opx/liq	Pl/liq	Mt/liq	Ap/liq
Cr	0·7	6	10	0·01	32	0·01
Ni	5	2	5	0·01	10	0·01
Rb	0·01	0·02	0·02	0·07	0·01	0·56
Ba	0·01	0·02	0·01	0·23	0·01	0·95
Sr	0·01	0·06	0·04	1·8	0·01	1·67
Nb	0·01	0·005	0·15	0·01	0·4	0·09
Zr	0·01	0·1	0·18	0·048	0·1	0·01
Y	0·01	0·9	0·18	0·03	0·2	5·08
La	0·007	0·06	0·02	0·15	0·53	5·16
Ce	0·007	0·1	0·02	0·1	0·56	6·34
Nd	0·007	0·23	0·03	0·08	0·55	6·6

Ol, olivine; Cpx, Ca-rich pyroxene; Opx, orthopyroxene; Pl, plagioclase; Mt, magnetite; Ap, apatite.

εSr–εNd relationships (Fig. 10) reveal that the HTi-D2 tholeiitic dyke A38 and the calc-alkaline andesitic D3 dykes plot in the enriched quadrant with respect to BE, suggesting an EMI-type isotopic signature, similar to the Florida (Uruguay) and Uauà (Brazil, São Francisco craton) Proterozoic tholeiitic dykes. Conversely, and particularly for sample A4, the LTi-D1 tholeiitic dykes plot in the enriched quadrant in terms of εSr, but in the depleted one in terms of εNd.

PETROGENESIS

Crystal fractionation

A possible mechanism for interdyke differentiation is fractional crystallization. This process was tested by performing MELTS (Ghiorso & Sack, 1995) and XLFRAC (Stormer & Nicholls, 1978) major element modelling. MELTS can model the crystal fractionation process of a magma on the basis of its major element composition, total pressure, fO_2 and water content. A Rayleigh fractionation model was then tested to compare calculated vs observed trace element contents (Tables 9–12), using the solid–liquid partition coefficients listed in Table 8.

MELTS results indicate that the mineral compositional variation of D1 LTi tholeiites is compatible with olivine/Ca-poor pyroxene + augite + plagioclase fractional crystallization at low pressure (0·1–0·4 GPa), low fO_2 (FMQ – 1 log unit) and H_2O <0·3 wt % (Fig. 11). Similarly, XLFRAC results (Table 9) indicate that differentiation from dykes with 8 wt % MgO (A5 and A25) to those with 6–7 wt % MgO (M.E.D1) is compatible with 27–32% removal of plagioclase (9–12%), augite (15–16%) and olivine (2%, A5) or orthopyroxene (6%, A25). In general, calculated/observed trace element values are satisfactory, with the exception of Rb and Ba. It should be noted that, starting from parental magma A5 (Rb and Ba 7 and 31 ppm, respectively), it is impossible to use fractional crystallization to match the Rb and Ba concentrations of the mean composition of the moderately evolved D1 dykes (i.e. M.E.D1: Rb 106 ppm, Ba 166 ppm), probably as a result of alteration that did not affect elements less sensitive to alteration (e.g. Zr, Nb).

D1a LTi tholeiitic dykes, characterized by high REE, Zr, Y and Nb contents, require parental magmas enriched in these elements. Among the D1 dykes with 8 wt % MgO, only sample A32 has the high content of incompatible elements. XLFRAC calculations (Table 10) indicate that this transition from A32 to the mean composition of D1a dykes is compatible with 47% fractionation of olivine (11%), clinopyroxene (8%), plagioclase (24%) and magnetite (4%). Calculated/observed trace element values are broadly consistent with such a differentiation process. The MELTS program (Fig. 11) indicates that this fractional crystallization may have occurred at low fO_2 (FMQ – 1 log unit) and 0·1 GPa pressure, in near-anhydrous conditions (H_2O 0·1 wt %).

MELTS modelling for the D2 HTi tholeiites (Fig. 11) indicates pigeonite as the dominant fractionating phase, at both 'high' (0·8 GPa) and low (0·1 GPa) pressures, for low H_2O (0·1 wt %) and fO_2 (FMQ – 1 log unit) conditions. XLFRAC mass balances, in conjunction with calculated/observed trace element

Table 9: Mass balance calculations (Stormer & Nicholls, 1978) for fractional crystallization transition from less (A5, A25) to the mean of the more evolved (M.E.D1) D1 tholeiitic dykes (see text for explanation)

	A5	M.E.D1	OL(83)	CPX	PL(71)		A5	calc.	calc./obs.
SiO_2	50·72	50·51	39·93	52·56	50·17	Cr	356	157	0·82
TiO_2	0·99	1·15	0·00	0·09	0·05	Ni	147	122	1·01
Al_2O_3	14·66	16·02	0·00	0·35	31·52	Rb	7	10	0·09
FeO_{tot}	10·72	11·51	14·32	11·40	0·60	Ba	31	42	0·25
MnO	0·18	0·18	0·00	0·21	0·00	Sr	138	155	0·91
MgO	8·02	6·71	45·00	13·09	0·00	Nb	5	7	1·39
CaO	12·24	10·15	0·74	22·18	14·30	Zr	74	100	1·13
Na_2O	2·17	2·29	0·00	0·13	3·34	Y	22	26	0·94
K_2O	0·19	1·36	0·00	0·00	0·02	La	5	7	0·94
P_2O_5	0·11	0·12	0·00	0·00	0·00	Ce	19	25	1·27
						Nd	10	13	1·11
wt %			2·26	15·96	9·23				
$\Sigma res^2 = 0·75$									
	A25	M.E.D1	OPX	CPX	PL(71)		A25	calc.	calc./obs.
SiO_2	51·34	50·51	53·28	51·90	50·17	Cr	157	37	0·20
TiO_2	0·87	1·15	0·30	0·52	0·05	Ni	110	78	0·64
Al_2O_3	14·69	16·02	0·94	2·06	31·52	Rb	96	140	1·32
FeO_{tot}	10·56	11·51	19·40	10·82	0·60	Ba	65	93	0·56
MnO	0·19	0·18	0·37	0·27	0·00	Sr	201	228	1·33
MgO	8·16	6·71	23·41	15·98	0·00	Nb	3	4	0·88
CaO	11·21	10·15	2·28	18·28	14·30	Zr	62	88	1·00
Na_2O	2·06	2·29	0·01	0·18	3·34	Y	20	25	0·92
K_2O	0·83	1·36	0·00	0·00	0·02	La	3	4	0·61
P_2O_5	0·09	0·12	0·00	0·00	0·00	Ce	13	19	0·93
						Nd	8	11	0·93
wt %			6·43	14·47	11·55				
$\Sigma res^2 = 0·33$									

In parentheses: forsterite and anorthite contents of olivine (OL) and plagioclase (PL); CPX, Ca-rich pyroxene; OPX, orthopyroxene; Calc., calculated; obs., observed; Σres^2, sum of squares of major element residuals.

values (Table 11), indicate that the transition from less evolved (MgO 7 wt %) to more evolved (MgO 4 wt %) tholeiites requires fractionation of pigeonite (19%) and plagioclase (8%).

The transition from the calc-alkaline D3 andesitic basalts (MgO 7 wt %) to andesites (MgO 4 wt %) requires removal of olivine or orthopyroxene. For the fractional crystallization of andesitic basalt T12, MELTS (Fig. 11) indicates that orthopyroxene is a liquidus phase even at 0·1 GPa [fO_2 = FMQ + 2 log unit, H_2O 1·0 wt %). Mass balance calculations and calculated/observed trace element abundances (Table 12) indicate that the transition from T12 (andesitic basalt) to A54 (andesite) is compatible with 26% removal of orthopyroxene (7%), clinopyroxene (5%), plagioclase (13%) and magnetite (1%).

XLFRAC results indicate that the silicic D4 dykes may derive from D3 andesites through 73% fractionation of clinopyroxene (36%), plagioclase (28%), magnetite (1%) and alkali-feldspar (8%), but there are great differences between calculated and observed trace element values (Table 12).

Variation diagrams (Figs 6 and 7) and Zr, La vs Ni relationships (Fig. 12) show that dykes D1, D1a,

Table 10: Mass balance calculations (Stormer & Nicholls, 1978) for the fractional crystallization transition from the less evolved D1 dyke (A32) with highest incompatible element contents (A32) to the mean of the tholeiitic D1a dykes (see text for explanation)

	A32	Mean D1a	OL(82)	CPX	PL(71)	MT		A32	calc.	calc./obs.
SiO_2	48·72	53·67	39·76	52·56	50·17	0·10	Cr	144	18	0·17
TiO_2	0·91	1·21	0·00	0·09	0·05	16·14	Ni	76	30	1·48
Al_2O_3	15·65	15·49	0·00	0·35	31·52	1·79	Rb	64	119	2·24
FeO_{tot}	12·46	11·50	15·21	11·40	0·60	81·20	Ba	318	561	0·73
MnO	0·2	0·18	0·00	0·21	0·00	0·70	Sr	302	321	0·97
MgO	8·44	4·72	44·28	13·09	0·00	0·04	Nb	10	19	1·37
CaO	9·66	8·26	0·74	22·18	14·30	0·02	Zr	96	177	0·92
Na_2O	2·3	2·92	0·00	0·13	3·34	0·00	Y	27	45	1·19
K_2O	1·22	1·71	0·00	0·00	0·02	0·00	La	12	21	0·53
P_2O_5	0·44	0·35	0·00	0·00	0·00	0·00	Ce	33	58	0·80
							Nd	18	31	0·84
wt %		11·07	8·43	23·57	4·46					
$\Sigma res^2 = 0·40$										

MT, magnetite; other abbreviations and notation as in Table 9.

Table 11: Mass balance calculations (Stormer & Nicholls, 1978) for the fractional crystallization transition from the less differentiated (A53) to the more evolved (A39) D2 tholeiitic dykes (see text for explanation)

	A53	A39	PIG	PL(71)		A39	calc.	calc./obs.
SiO_2	49·58	48·11	53·59	50·17	Cr	58	24	0·41
TiO_2	2·14	3·61	0·19	0·05	Ni	24	34	1·43
Al_2O_3	13·06	13·99	1·06	31·52	Rb	47	46	0·97
FeO_{tot}	15·25	15·83	17·46	0·60	Ba	976	633	0·65
MnO	0·23	0·22	0·47	0·00	Sr	488	419	0·86
MgO	6·72	3·87	21·81	0·00	Nb	51	20	0·39
CaO	8·71	9·17	5·41	14·30	Zr	415	267	0·64
Na_2O	2·25	2·05	0·02	3·34	Y	66	48	0·73
K_2O	0·90	1·63	0·00	0·02	La	48	65	1·36
P_2O_5	1·16	1·52	0·00	0·00	Ce	96	122	1·27
					Nd	58	74	1·27
wt %		18·53	7·89					
$\Sigma res^2 = 0·88$								

PIG, pigeonite; other abbreviations and notation as in Table 9.

D2 and D3 are related to different parental magmas.

Primary magma compositions for these dykes (P-D1, P-D1a, P-D2 and P-D3, respectively; Table 13) were calculated starting from samples A5 (*mg*-number 60), A32 (*mg*-number 58), A53 (*mg*-number 53) and T12 (*mg*-number 62), respectively, by adding olivine, clinopyroxene and orthopyroxene (in proportions 5:3:1, respectively) to achieve *mg*-number values of 72–73. Plagioclase was not included as fractionating phase, because the MELTS results (Fig. 11) show that

Table 12: Mass balance calculations (Stormer & Nicholls, 1978) for the fractional crystallization transition from the less differentiated (T12) to the more evolved (A54) D3 calc-alkaline dykes, and to silicic (A51) D4 dykes (see text for explanation)

	T12 (D3)	A54 (D3)	OPX	CPX	PL(60)	MT		A54	calc.	calc./obs.
SiO_2	58·03	59·77	53·28	54·06	52·98	0·14	Cr	45	97	2·16
TiO_2	0·77	0·78	0·30	0·05	0·06	22·66	Ni	12	24	2·00
Al_2O_3	13·33	14·57	0·94	0·29	29·72	2·32	Rb	154	84	0·55
FeO_{tot}	8·58	8·52	19·40	5·88	0·28	74·66	Ba	517	617	1·19
MnO	0·18	0·16	0·37	0·21	0·00	0·02	Sr	375	583	1·55
MgO	7·00	3·68	23·41	14·79	0·00	0·04	Nb	9	7	0·78
CaO	8·05	6·28	2·28	24·46	12·17	0·17	Zr	135	173	1·28
Na_2O	2·49	3·75	0·01	0·26	4·33	0·00	Y	29	28	0·97
K_2O	1·28	2·17	0·00	0·00	0·47	0·00	La	28	39	1·39
P_2O_5	0·29	0·32	0·00	0·00	0·00	0·00	Ce	64	83	1·30
Total	100·00	100·00	99·99	100·00	100·01	100·01	Nd	34	42	1·24
wt %		6·78	4·84	13·01	1·33					
$\Sigma res^2 = 0·19$										

	A54 (D3)	A51(D4)	CPX	PL(35)	AF	MT		A51	calc.	calc./obs.
SiO_2	59·77	76·21	48·06	59·97	64·02	0·14	Cr	2	2	1·00
TiO_2	0·78	0·11	0·96	0·00	0·03	22·66	Ni	5	11	2·20
Al_2O_3	14·57	12·72	7·08	25·34	18·93	2·32	Rb	141	349	2·48
FeO_{tot}	8·52	1·88	21·42	0·00	0·30	74·66	Ba	802	1590	1·98
MnO	0·16	0·03	0·62	0·00	0·00	0·02	Sr	178	292	1·64
MgO	3·68	0·17	8·84	0·00	0·00	0·04	Nb	11	31	2·82
CaO	6·28	1·30	12·06	6·91	0·68	0·17	Zr	169	436	2·58
Na_2O	3·75	3·84	0·95	7·76	0·63	0·00	Y	26	57	2·19
K_2O	2·17	3·72	0·00	0·02	15·41	0·00	La	56	91	1·63
P_2O_5	0·32	0·02	0·00	0·00	0·00	0·00	Ce	107	204	1·91
Total	100·00	100·00	99·99	100·00	100·00	100·01	Nd	49	102	2·08
wt %		35·85	28·27	8·29	0·77					
$\Sigma res^2 = 0·68$										

MT, magnetite; AF, alkali feldspar; other abbreviations and notation as in Table 9.

plagioclase is not a liquidus phase in the early stages of crystal fractionation, even at low pressure. The relatively low Cr and Ni contents do not take account of sulfide (pyrite, pyrrotine, calc-pyrite, pentlandite) fractionation (Echeveste & Fernandez, 1994).

Crustal contamination

In general, the Azul and Tandil dykes have Sr_i higher than that of BE. The calc-alkaline D3 and D4 dykes are characterized by IE and Sr_i values (0·7029–0·7050) lower than or similar to those of the 'old granitoids' (0·7034–0·7060; Varela *et al.*, 1988) and therefore crustal contamination is not easy to detect. D1 and D2 tholeiitic dykes have Sr_i ratios ranging from 0·7031 to 0·7111. Figure 13 reveals that Sr_i increases in both D1 and D2 dykes are not correlated with SiO_2, MgO, K_2O, Rb, Ba, La, Zr and Nb. It should be noted that the country rocks have Sr_i ratios <0·7070 and cannot represent end-members in terms of simple mixing. Therefore, we modelled AFC contamination (DePaolo, 1981) for D1 and D2 dykes assuming the 'old' and 'young granitoids' of Varela *et al.* (1988) as contaminants and as starting compositions those of the D1 (A2, A5) and D2 (A53, A38) dykes with the lowest Sr_i values. Calculations were carried out with bulk D(Sr) partition

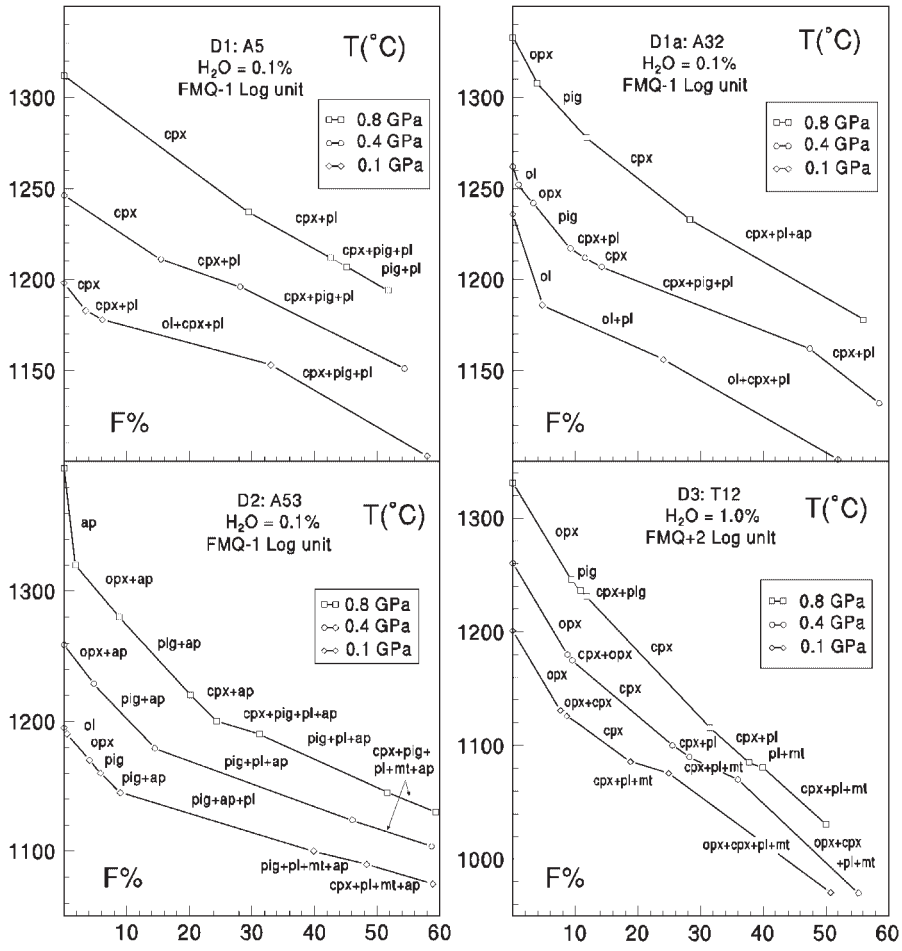

Fig. 11. Percentages of solid removal (F%) vs temperature (T°C) according to the MELTS fractional crystallization model of Ghiorso & Sack (1995) for the Azul and Tandil dyke swarms. ol, olivine; opx, orthopyroxene; cpx, augite; pig, pigeonite; pl, plagioclase; ap, apatite; mt, magnetite. FMQ, fayalite–magnetite–quartz buffer. (See text for explanation.)

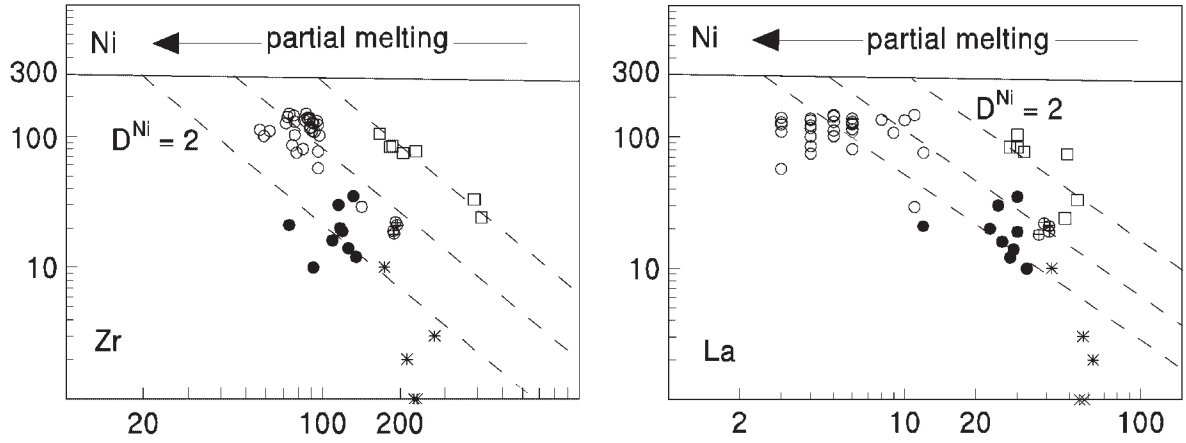

Fig. 12. Log La and Zr (ppm) vs log Ni (ppm) for the Azul and Tandil dyke swarms. Symbols as in Fig. 7. Dashed straight lines: crystal fractionation trends for bulk D^{Ni} partition coefficient = 2. It should be noted that, assuming the same parental source mantle, D1 dykes were generated by a lower melting degree for Ni–Zr but not for Ni–La ratios relative to D3 dykes.

Table 13: Calculated 'primary' compositions of D1 (P-D1), D1a (P-D1a), D2 (P-D2) and D3 (P-D3) dykes, starting from the bulk-rock compositions of A5, A32, A53 and T12, respectively

	P-D1	P-D1a	P-D2	P-D3	OL (89)	CPX	OPX
SiO_2	49·71	48·03	48·45	56·25	40·69	52·50	56·23
TiO_2	0·81	0·72	1·43	0·68	0·00	0·36	0·00
Al_2O_3	11·92	12·13	8·98	11·60	0·00	3·71	1·71
FeO_{tot}	10·38	11·60	13·10	8·65	10·71	6·00	10·53
MnO	0·14	0·15	0·15	0·15	0·00	0·00	0·00
MgO	13·87	15·35	17·12	11·31	48·60	17·62	31·53
CaO	11·21	9·04	7·95	7·89	0·00	19·67	0·00
Na_2O	1·73	1·74	1·48	2·14	0·00	0·14	0·00
K_2O	0·15	0·92	0·58	1·09	0·00	0·00	0·00
P_2O_5	0·09	0·33	0·75	0·25	0·00	0·00	0·00
mg-no.	72·92	72·80	72·55	72·56			
Cr	600	269	439	503			
Ni	288	174	270	56			
Rb	6	48	22	54			
Ba	25	240	312	406			
Sr	110	229	241	489			
Nb	4	8	10	4			
Zr	59	73	137	114			
Y	19	22	28	20			
La	3	9	32	26			
Ce	8	25	60	54			
Nd	6	14	37	28			

Primary compositions were calculated to match at. 100 × Mg/(Mg + Fe^{2+}) of 73. The following mineral amounts were added: P-D1, A5 + 15% OL + 10% CPX + 1·5% OPX; P-D1a, A32 + 19% OL + 12% CPX + 2% OPX; P-D2, A53 + 30% OL + 18% CPX + 6% OPX; P-D3, T12 + 10% OL + 6% CPX + 1% OPX. Abbreviations and notation as in Table 9.

coefficients of 0·5 and 0·9, considering that plagioclase was not a liquidus phase in the earliest stages of differentiation (Fig. 11). The results (Fig. 14) indicate that Sr_i variations in both LTi-D1 and HTi-D2 dykes are compatible with assimilation of small amounts (r = 0·2) of both 'young' and 'old granitoids' (Cavazzini, 1996). It should be noted, however, that D1 and D2 dykes with Sr_i values >0·707 do not conform to AFC mixing curves, even for residual liquid fractions as low as 0·2–0·3. This suggests that alteration may have contributed towards reaching the highest Sr_i values. In summary, major and trace elements, mass balance calculations and isotopic data all indicate that D1 and D2 tholeiitic dykes with Sr_i <0·7050 were not significantly affected by crustal contamination.

Source mantle

The melting degree for the 'primary' D1 to D3 basalts was calculated (XLFRAC) using a peridotitic major element composition from Ringwood (1966; pyrolite), Chen (1971) and Ionov & Hofmann (1995). Calculations were carried out for dry and amphibole-bearing spinel- and garnet-peridotite mineral assemblages. The results (Table 14) indicate that the highest degrees of melting (15–9% and 14–6% for garnet and spinel peridotites) refer to the calc-alkaline D3 dykes, whereas the lowest ones (7–3% and 6–4%: garnet and spinel peridotites, respectively) apply to the high-TiO_2 D2 tholeiitic dykes (Fig. 15).

Incompatible trace elements (IE) in the peridotitic sources (Table 15) were computed (batch melting; Hanson, 1978) using the partition coefficients of Table 16 and the calculated degrees of melting and solid residua (Table 14). The multi-elemental diagrams of Fig. 16 reveal that the IE of D1 peridotitic sources are depleted with respect to PM of Sun & McDonough (1989), irrespective of whether such sources are enriched (i.e. pyrolite) or relatively depleted in terms of major

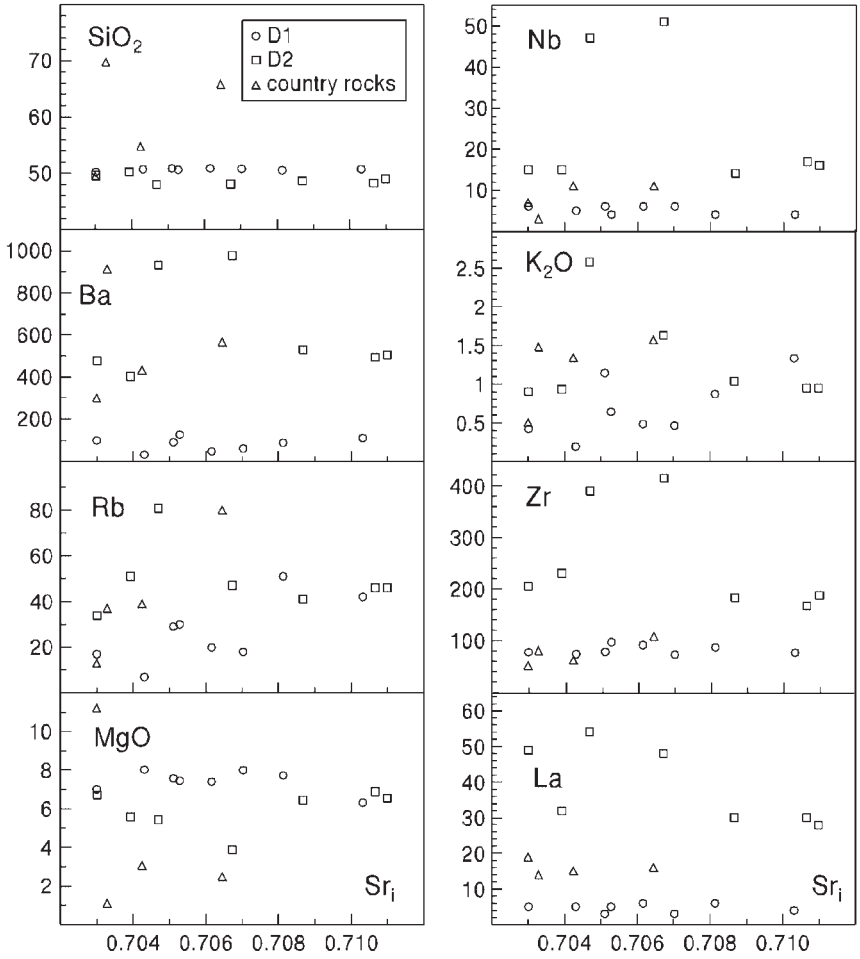

Fig. 13. Initial (1565 Ma) $^{87}Sr/^{86}Sr$ (Sr_i) ratios vs MgO, K_2O and SiO_2 (wt %), and Rb, Ba, La, Zr and Nb (ppm).

elements. The relatively low IE contents of a major-element pyrolite-type mantle indicate that IE depletion of such peridotites reflects a low degree (e.g. <1%) of melting, which did not significantly change the original mineral assemblage or major element composition. D1a sources (Fig. 16b) have IE higher than D1 sources, are especially enriched in Rb, Ba and K, and display negative Nb and Sr spikes and positive P spikes. D2 source patterns (Fig. 16c) are similar to those of D1a and have distinct P and Ti positive spikes, as well as a more pronounced Sr negative anomaly. D3 source patterns (Fig. 16d) are globally enriched with respect to PM and are characterized by high Nb and less marked Ti negative anomalies. The high (LILE, LREE)/(HFSE, HREE) values of D3 calc-alkaline dykes with respect to D1 tholeiitic dykes do not necessarily imply different mantle peridotite residua, i.e. garnet- vs spinel-peridotites (see Fig. 15 for melting degrees). Such incompatible element ratio differences may reflect LILE–LREE enrichment in D3 mantle source as a result of 'fluid/small-volume melts' metasomatism that may have occurred in Archaean–Proterozoic times [T_{DM}(Nd) ~2·5 Ga].

DISCUSSION AND CONCLUSIONS

Early Proterozoic dykes

The oldest Precambrian dyke magmatism of the Rio de La Plata craton outcrops in Argentina (Tandil region) and is dated at 2·0 Ga. The dykes crosscut the crystalline basement and are sub-coeval with the youngest 'old granitoids' that intruded the basement (2·2–2·0 Ga). This magmatism (andesites: D3; rhyolites: D4), intruded during the transtensional stages of the Transamazonian Orogeny, has calc-alkaline geochemical features including negative Nb–Ti spikes. The calculated D3 primary andesite magmas may be derived (major elements) from either anhydrous or amphibole-bearing peridotites by 5–15% batch melting, in the

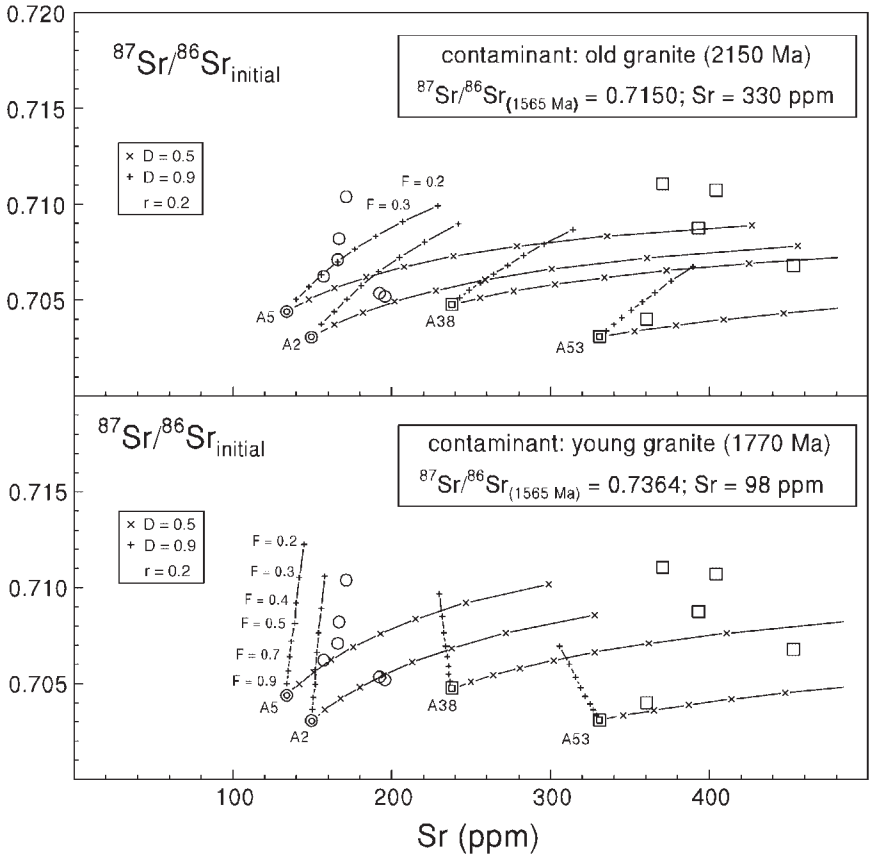

Fig. 14. Sr (ppm) vs initial $^{87}Sr/^{86}Sr$ for D1 (○) and D2 (□) tholeiitic LTi and HTi, respectively, dykes from the Azul and Tandil regions. Curves calculated according to the AFC crustal contamination model of DePaolo (1981). *D*, bulk Sr partition coefficient; *r*, rate of assimilated/crystallized materials; *F*, liquid fraction. Contaminants: 'old granitoids' is sample 99 of Varela *et al.* (1988); 'young granitoids' is sample 40 of Varela *et al.* (1988).

spinel and garnet facies. The high LREE/HREE ratios of the D3 dykes are compatible with garnet-peridotite residua as well as with spinel peridotites enriched in LREE by 'metasomatic processes' involving fluids and/or small-volume melts related to peridotites contaminated by eclogite-derived melts (see Rivalenti *et al.*, 1998). These 'metasomatic processes' imply interaction with subducted rutile-bearing crustal material (e.g. Ryerson & Watson, 1987; Brenan *et al.*, 1994) and possibly ilmenite in the residua (Ayers *et al.*, 1997; Ayers, 1998). The anhydrous primary mineral assemblages of the andesitic dykes indicate that melting occurred in near-anhydrous water-undersaturated conditions. The transition from andesites to rhyolites (major and trace elements) is only partly consistent with fractional crystallization.

The initial Sr isotopic ratios of the andesites and rhyolites are similar to those of the country rocks and the 'old granitoids', and are higher than that of BE; crustal contamination was not appreciable. In terms of εSr and εNd, these dykes, as well as those of Uauà (São Francisco craton, Brazil, 2·2–2·0 Ga), plot in the enriched quadrant and trend towards the EMI mantle component of Hart & Zindler (1989). Assuming that the Sm/Nd ratio was not significantly changed by melting, the T_{DM}(Nd) of these Argentinian dykes indicate that they could be related to source mantle that underwent metasomatic processes responsible for their EMI Sr–Nd isotopic signature in Archaean–Proterozoic times (~2·5 Ga).

Middle Proterozoic dykes

The youngest Precambrian dyke magmatism of the Rio de La Plata craton in Argentina (Azul and Tandil regions) dates at ~1·6 Ga, an age similar to that (1·7–1·8 Ga; Bossi *et al.*, 1993; Teixeira *et al.*, 1999) of the oldest dykes from Uruguay (Florida region). The Argentina dyke swarms intrude both the 'old' and 'young granitoids' and have compositional characteristics typical of tholeiitic suites, with low and high

Table 14: Weight per cent mineral assemblages calculated (Stormer & Nicholls, 1978) from peridotite compositions of Ringwood (1966; P1 and P2), Chen (1971; P3 and P4) and Ionov & Hofmann (1995; P5 and P6), and mineral assemblages of residua after extraction of P-D1, P-D1a, P-D2 and P-D3 primary magmas (see text for explanation)

	Peridotites					
	P1	P2	P3	P4	P5	P6
OL	56·23[1]	49·52[1]	65·28[1]	65·22[1]	55·98[2]	59·78[2]
OPX	15·61[3]	28·87[3]	18·38[1]	18·99[1]	26·94[2]	20·28[2]
CPX	16·35[3]	17·20[3]	10·17[1]	9·16[1]	13·78[2]	14·24[4]
GT	11·81[1]		6·16[1]	4·35[1]		
SP		4·42[3]			4·30[2]	2·84[2]
AMP				2·03[5]		2·86[4]
Σres^2	0·62	0·59	0·06	0·04	0·41	0·16
D1 residua						
OL	67·41	64·01	73·45	73·01	63·08	64·48
OPX	17·58	24·27	18·33	18·40	22·79	18·85
CPX	8·93	9·50	7·02	7·07	10·75	11·79
GT	6·08		1·20	1·25		
SP		2·23			3·38	2·37
AMP				0·26		2·51
Σres^2	0·44	0·50	0·02	0·02	0·12	0·01
F	13·09	13·06	8·76	8·34	7·06	5·40
D1a residua						
OL	64·39	60·28	70·70	70·72	61·81	63·58
OPX	16·95	24·20	18·47	18·45	23·09	19·07
CPX	12·30	13·08	8·61	8·61	11·70	12·94
GT	6·37		2·23	2·23		
SP		2·44			3·40	2·45
AMP						1·95
Σres^2	0·43	0·49	0·01	0·01	0·11	0·01
F	10·75	10·25	6·45	6·46	6·19	4·67
D2 residua						
OL	60·60	52·75	67·87	67·53	60·17	62·48
OPX	15·89	27·38	18·22	18·39	27·78	19·47
CPX	14·20	16·01	9·43	9·26	12·27	13·49
GT	9·31		4·49	4·24		
SP		3·87			3·77	2·72
AMP				0·58		1·84
Σres^2	0·44	0·55	0·02	0·02	0·12	0·01
F	6·57	5·69	3·40	2·98	5·06	3·84
D3 residua						
OL	75·49	71·28	78·32	76·96	66·86	66·94
OPX	4·42	12·06	12·36	13·05	17·93	15·85
CPX	13·57	14·21	8·47	8·62	11·74	13·73
GT	6·52		0·85	1·36		
SP		2·45			3·48	2·75
AMP						0·73
Σres^2	0·34	0·39	0·01	0·01	0·08	0·01
F	13·09	13·06	8·76	8·34	7·06	5·40

[1]MacGregor (1974); [2]Ionov & Hofmann (1995); [3]Ringwood (1966); [4]Takazawa *et al.* (1996); [5]Wilkinson & Le Maitre (1987). OL, olivine; OPX, orthopyroxene; CPX, Ca-rich pyroxene; GT, garnet; SP, spinel; AMP, amphibole; *F*, percentage of liquid fraction; Σres^2, sum of squares of major element residuals.

Table 15: Calculated incompatible element (batch melting; Hanson, 1978) mantle sources, for tholeiitic (P-D1, P-D1a, P-D2) and calc-alkaline (P-D3) calculated primary magmas from the Azul and Tandil regions

	P1	P2	P3	P4	P5	P6
P-D1 sources						
Rb	0·79	0·79	0·53	0·51	0·43	0·38
Ba	3·28	3·27	2·20	2·12	1·78	1·60
K	207·31	206·90	138·88	136·02	112·47	123·87
Nb	0·53	0·53	0·36	0·35	0·29	0·30
La	0·41	0·41	0·27	0·26	0·23	0·19
Ce	1·10	1·10	0·75	0·72	0·64	0·56
Sr	15·24	15·30	10·35	9·92	8·77	7·30
Nd	0·89	0·88	0·61	0·59	0·54	0·51
P	69·61	67·74	46·23	44·50	40·07	34·67
Zr	9·59	8·81	6·16	5·97	5·39	4·90
Ti	1321·04	1205·47	903·49	892·94	902·86	894·35
Y	5·17	3·39	2·75	2·70	2·40	2·21
P-D1a sources						
Rb	5·21	4·99	3·15	3·15	3·04	2·59
Ba	25·89	24·70	15·57	15·60	14·95	13·09
K	825·47	789·36	497·09	497·85	478·84	505·47
Nb	0·87	0·83	0·53	0·53	0·51	0·51
La	1·01	0·98	0·62	0·62	0·61	0·51
Ce	2·87	2·82	1·79	1·79	1·79	1·56
Sr	26·13	25·67	16·32	16·34	16·27	13·44
Nd	1·76	1·75	1·14	1·14	1·16	1·09
P	175·66	167·93	109·22	109·37	109·14	93·78
Zr	10·01	9·00	6·18	6·18	6·02	5·41
Ti	870·42	817·47	613·18	613·47	638·20	625·63
Y	5·55	3·62	3·24	3·24	2·68	2·48
P-D2 sources						
Rb	2·46	1·74	1·27	1·21	1·71	1·47
Ba	25·73	18·17	13·30	12·69	17·83	15·78
K	410·57	299·14	212·04	213·91	284·66	306·98
Nb	0·88	0·64	0·46	0·45	0·61	0·62
La	1·70	1·24	0·90	0·85	1·20	1·01
Ce	4·35	3·28	2·34	2·23	3·12	2·75
Sr	26·34	19·81	14·27	13·40	19·06	15·91
Nd	2·73	2·13	1·54	1·49	1·96	1·87
P	276·17	199·94	150·41	142·81	190·17	165·38
Zr	13·66	9·13	7·58	7·31	8·55	7·78
Ti	1588·77	1249·69	1035·67	1024·57	1121·96	1104·56
Y	5·13	2·34	2·88	2·80	2·08	1·96
P-D3 sources						
Rb	8·03	7·86	5·29	4·98	4·34	3·34
Ba	59·89	58·61	39·49	37·13	32·23	24·91
K	1339·59	1311·02	881·87	829·50	721·75	597·32
Nb	0·60	0·58	0·39	0·37	0·32	0·26
La	4·00	3·92	2·63	2·48	2·20	1·73
Ce	8·50	8·35	5·59	5·29	4·76	3·85
Sr	75·99	74·86	50·34	47·59	42·77	33·73
Nd	4·78	4·65	3·13	2·98	2·76	2·38
P	179·97	172·46	115·98	110·39	100·63	81·70
Zr	20·45	18·58	12·70	12·24	11·16	9·33
Ti	978·11	886·50	640·50	634·73	637·91	598·60
Y	6·04	4·02	2·99	3·07	2·68	2·45

P1 to P6 as in Table 14. (See text for explanation.)

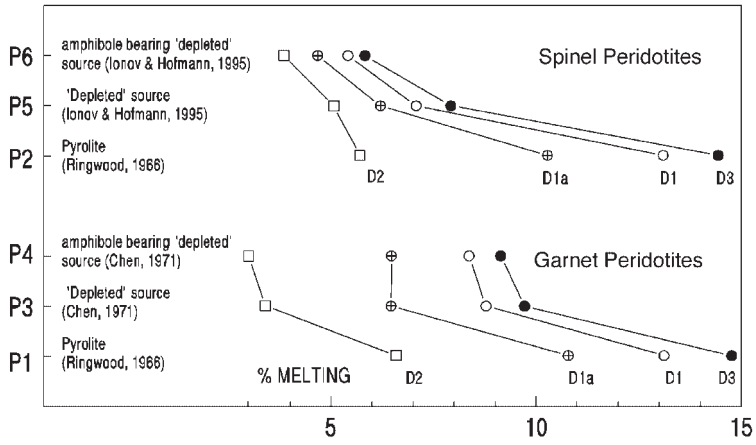

Fig. 15. Melting degrees for tholeiitic (D1, D1a and D2) and calc-alkaline (D3) calculated primary magmas for anhydrous and amphibole-bearing source mantle in the spinel and garnet-facies. (See text for explanation.)

Table 16: Mineral/liquid partition coefficients used for melting modelling

	Ol/liq	Opx/liq	Cpx/liq	Gt/liq	Sp/liq	Amp/liq
Rb	0·00018	0·0006	0·011	0·0007	0·0001	0·3
Ba	0·00032	0·00069	0·0007	0·00001	0·00001	0·4
K	0·000001	0·00001	0·0072	0·00001	0·000001	1
Nb	0·0001	0·003	0·0077	0·01	0·01	0·8
La	0·000007	0·0005	0·0536	0·01	0·0006	0·17
Ce	0·00001	0·0009	0·0858	0·004	0·0006	0·26
Sr	0·00019	0·007	0·067	0·0011	0·005	0·12
Nd	0·00007	0·009	0·173	0·057	0·0006	0·44
P	0·0008	0·004	0·1	0·1	0·05	0·2
Zr	0·0007	0·02	0·1234	0·3	0·07	0·35
Ti	0·015	0·14	0·384	0·6	0·15	0·69
Y	0·001	0·06	0·4	1·9	0·07	0·2

Source data from McKenzie & O'Nions (1991) and Kelemen *et al.* (1993). Ol, olivine; Cpx, Ca-rich pyroxene; Opx, orthopyroxene; Gt, garnet; Sp, spinel; Amp, amphibole.

TiO_2 contents (LTi and HTi, respectively). Most LTi tholeiites (D1 dykes) have REE patterns similar to those of E-MORB, except for a few tholeiitic andesitic basalts (D1a dykes) characterized by higher LREE/HREE ratios (e.g. $La/Yb_{CN} \sim 7$). D1 dykes have slightly positive or negative Nb spikes and HREE lower than those of E-MORB, whereas D1a dykes have a distinct negative Nb spike. The dykes with high TiO_2 and incompatible elements (D2) are characterized by high LREE/HREE and slightly positive or negative Nb spikes. The Middle Proterozoic dykes cannot be related to the same parental magma, but require different primary melts originating from different mantle sources. The genesis of D1 tholeiites requires 5–13% melting of peridotites depleted in incompatible elements relative to PM; that of D1a (5–11% melting) and D2 (3–7% melting) dykes would be related to source mantle enriched in LILE and LREE with respect to PM. The tholeiitic dykes that can be considered unaffected by appreciable crustal contamination are characterized by initial $^{143}Nd/^{144}Nd$ ranging from slightly lower to higher than BE (D2 and D1 dykes, respectively).

In summary, petrological, geochemical and Sr–Nd isotope data support the hypothesis that the various Middle Proterozoic tholeiitic dykes require distinct mantle sources, ranging from IE-depleted (basalt melt extraction) to IE-enriched ('metasomatic processes')

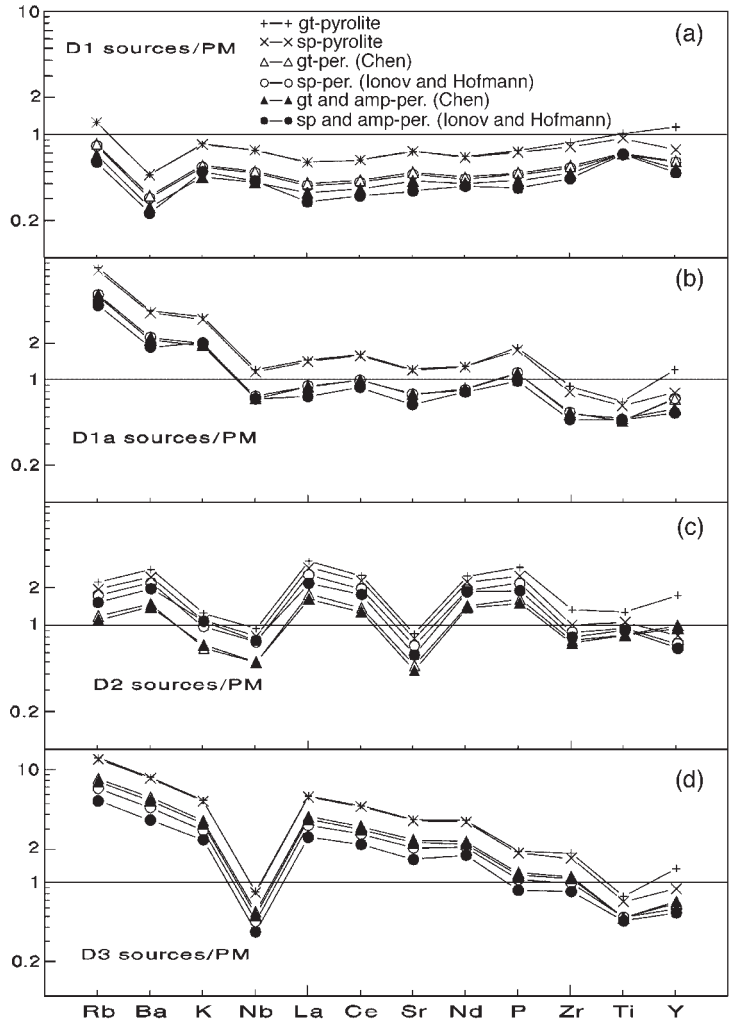

Fig. 16. Multi-elemental plots of calculated (batch melting; Hanson, 1978) mantle sources, normalized to Primitive Mantle (PM) of Sun & McDonough (1989), for tholeiitic (D1, D1a, D2) and calc-alkaline (D3) calculated primary magmas from the Azul and Tandil regions. (See text for explanation.)

peridotites. It should be noted that, in a very restricted area, particularly in Tandil (Fig. 2), both calc-alkaline and tholeiitic dykes occur; this indicates important small-scale mantle heterogeneity.

Lastly, it is notable that the Middle Proterozoic tholeiitic dykes from Uruguay (Florida region, Rio de La Plata craton) have geochemical features (mainly trace elements) similar to their D1 Argentina analogues (Figs 6 and 7).

Tectonic implications

The Early Proterozoic calc-alkaline dykes of Tandil are sub-coeval (~2·0 Ga) with the youngest intrusion of 'old granitoids' and represent transtensional stages of the Transamazonian Orogeny. On the other hand, the emplacement of Middle Proterozoic tholeiitic dykes in the Azul and Tandil regions relates to the development of the Rio de La Plata craton, where these dykes are sub-coeval (~1·6 Ga) with the youngest intrusion of the 'young granitoids' and are associated with extensional tectonics during a post-collisional Transamazonian stage (Dalla Salda *et al.*, 1988, 1992), 300–400 m.y. after the end of the Transamazonian Orogeny. Rogers (1996) proposed a time of 2·0 Ga for the existence of the 'Atlantica' continent, which includes the cratons of Amazonia (Guaporè and Guyana), São Francisco, Congo–Kasai, West Africa and, possibly, West Nile and Rio de La Plata. In our opinion, Rogers' reconstruction should take into consideration the spatial position of the southwestern Africa region. Volcanic and granitic rocks from the 'Richtersveld Subprovince', within the Namaqua Fold

Belts facing the Rio de La Plata craton in the Gondwana reconstruction (Fig. 1), have been related to the Eburnean Orogeny at ~2·0 Ga (Hartnady *et al.*, 1985; Reid, 1997) and are, therefore, coeval with the calc-alkaline rocks of Tandil and Azul. The African calc-alkaline rocks were subjected to metamorphic processes related to the Kibaran Orogeny (1·2–1·0 Ga; Hartnady *et al.*, 1985; Reid, 1997; Colliston & Schoch, 1998), but not appreciable in the corresponding Argentinian rocks. Also, within the Namaqua fold belts, in the Witberg–Aggeneys–Gamsberg ore district, metamorphosed basic tholeiites similar to the Tandil and Florida dykes are present whose emplacement occurred at 1·6–1·7 Ga (Reid *et al.*, 1987). The metamorphism of the African basalts (amphibolite facies) has been related to the Kibaran Orogeny (Reid, 1997). The similarities between the Proterozoic calc-alkaline and tholeitic rocks of Rio de La Plata and the southwestern Africa analogues suggest that these two regions were contiguous in Early Proterozoic as well as in Late Proterozoic times, consistent with the common sedimentary basin of La Tinta and Nama Groups (Dalla Salda, 1982).

In a global context, the generation of juvenile crust ('granitoids') within the Rio de La Plata craton occurred from 2·2 to 1·6 Ga. This time broadly corresponds to that attributed to the development of the Early Proterozoic Supercontinent proposed by Condie (1998) on the basis of the occurrence of greenstone belts. Yale & Carpenter (1998) partly confirmed this hypothesis, emphasizing the absence of giant dyke swarms in the periods that preceded and followed 2·4–2·2 and 1·6–1·4 Ga, respectively. These time gaps may well represent periods of continental dispersal after supercontinent break-up.

ACKNOWLEDGEMENTS

Special thanks are due to A. Cundari and A. Marzoli for fruitful suggestions related to the manuscript, and to the constructive reviewer's comments and criticism. L. Furlan (Trieste University) and A. Giaretta and A. Carampin (Padova University) are acknowledged for the valuable technical collaboration in this research. The authors acknowledge the financial support by FAPESP and CNPq (Brazilian Agencies) and CNR and MURST (Italian Agencies).

REFERENCES

Ayers, J. (1998). Trace element modeling of aqueous fluid–peridotite interaction in the mantle wedge of subduction zones. *Contributions to Mineralogy and Petrology* **132**, 390–404.

Ayers, J. C., Dittmer, S. K. & Layne, G. D. (1997). Partitioning of elements between peridotite and H_2O at 2·0–3·0 GPa and 900–1100°C, and application to the models of subduction zone processes. *Earth and Planetary Science Letters* **150**, 381–398.

Baer, G. & Heimann, A. (1995). *Physics and Chemistry of Dykes*. Rotterdam: A. A. Balkema.

Bellieni, G., Piccirillo, E. M., Petrini, R., Girardi, V. A. V., Menzes Leal, A. B., Texeira, W., Bastos Leal, L. R., De Min, A., Comin Chiaromonti, P. & Tanner de Oliveira, M. A. F. (1995). Petrological and Sr–Nd evidence bearing on Early Proterozoic magmatic events of the subcontinental mantle: São Francisco craton (Uauà, NE-Brazil). *Contributions to Mineralogy and Petrology* **122**, 252–261.

Bossi, J., Campal, N., Civetta, L., Demarchi, G., Girardi, V. A. V., Mazzucchelli, M., Negrini, L., Rivalenti, G., Fragoso Cesar, A. R. S., Sinigoi, S., Texeira, W., Piccirillo, E. M. & Molesini, M. (1993). Early Proterozoic dike swarms from western Uruguay: geochemistry, Sr–Nd isotopes and petrogenesis. *Chemical Geology* **106**, 263–277.

Boynton, W. V. (1984). Cosmochemistry of the rare earth elements: meteorite studies. In: Henderson, P. (ed.) *Rare Earth Element Geochemistry*. (Developments in Geochemistry collection.) Amsterdam: Elsevier, pp. 63–114.

Brenan, J. M., Shaw, H. F., Phinney, D. L. & Reyerson, F. J. (1994). Rutile–aqueous fluid partitioning of Nb, Ta, Hf, Zr, U and Th: implications for high field strength element depletions in island-arc basalts. *Earth and Planetary Science Letters* **128**, 327–339.

Buddington, A. F. & Lindsley, D. H. (1964). Iron–titanium oxide minerals and synthetic equivalents. *Journal of Petrology* **5**, 310–357.

Carmichael, I. S. E. (1967). The iron–titanium oxides of salic rocks and their associated ferromagnesian silicates. *Contributions to Mineralogy and Petrology* **14**, 36–64.

Cavazzini, G. (1996). Degrees of contamination in magmas evolving by assimilation–fractional crystallization. *Geochimica et Cosmochimica Acta* **60**, 2049–2052.

Chen, J. C. (1971). Petrology and chemistry of garnet lherzolite nodules in kimberlite from South Africa. *American Mineralogist* **56**, 2098–2110.

Colliston, W. P. & Schoch, A. E. (1998). Tectonostratigraphic features along the Orange River in the western part of the Mesoproterozoic Namaqua mobile belt. *South African Journal of Geology* **101**, 91–100.

Condie, K. C. (1998). Episodic continental growth and supercontinents: a mantle avalanche connection? *Earth and Planetary Science Letters* **163**, 97–108.

Dalla Salda, L. (1981). Tandilia, un ejemplo de tectonica de transcurrencia en basamento. *Revista Asociacion Geologica Argentina* **36**, 204–207.

Dalla Salda, L. (1982). Nama–La Tinta y el inicio de Gondwana. *Acta Geologica Lilloana* **16**, 23–38.

Dalla Salda, L., Bossi, J. & Cingolani, C. (1988). The Rio de la Plata cratonic region of Southwestern Gondwanaland. *Episodes* **11**, 263–268.

Dalla Salda, L., Franzese, J. R. & Posadas, V. G. (1992). The 1800 Ma mylonite–anatectic granitoid association in Tandilia, Argentina. *Basement Tectonics* **7**, 161–174.

DePaolo, D. J. (1981). Trace element and isotopic effects of combined wall rock assimilation and fractional crystallization. *Earth and Planetary Science Letters* **53**, 189–202.

Echeveste, H. & Fernandez, R. (1994). Asociaciones de oxidos y sulfuros en diques basicos de Las Sierras de Tandil, Provincia de Buenos Aires. *Revista del Museo de La Plata (Nueva Serie)* **11**, 99–118.

Fernández, R. R. & Echeveste, H. J. (1995). Caracterización geoquímica y petrológica de diques del Sistema de Tandilia, prov. de Buenos Aires. Argentina. *IV Jornadas Geológicas y Geofísicas Bonaerenses, Actas* **1**, 329–337.

Ghiorso, M. S. & Sack, R. O. (1995). Chemical mass transfer in magmatic processes IV. A revised and internally consistent thermodynamic model for the interpolation and extrapolation of liquid–solid equilibria in magmatic system at elevated temperatures and pressures. *Contributions to Mineralogy and Petrology* **119**, 197–212.

Girardi, V. A. V., Mazzucchelli, M., Molesini, M., Civetta, L., Petrini, R., Bossi, J., Campal, N., Teixeira, W. & Correia, C. T. (1996). Petrology and geochemistry of mafic dyke swarm of Treinta Y Tres Region, Northeast Uruguay. *Journal of South American Earth Sciences* **9**, 243–249.

Govindaraju, K. & Mevelle, G. (1987). Fully automated dissolution and separation methods for inductively coupled plasma atomic emission spectrometry rock analysis. Application to the determination of rare earth elements. *Journal of Analytical Atomic Spectrometry* **2**, 615–621.

Halls, H. C. & Fahrig, W. F. (eds) (1987). *Mafic Dyke Swarms. Geological Association of Canada, Special Paper* **34**, 503 pp.

Hanson, G. N. (1978). The application of trace elements to the petrogenesis of igneous rocks of granitic composition. *Earth and Planetary Science Letters* **38**, 26–43.

Hart, S. R. & Zindler, A. (1989). Constraints on the nature and development of chemical heterogeneities in the mantle convection. In: Peltier, W. R. (ed.) *Mantle Convection; Plate Tectonics and Global Dynamics*. New York: Gordon & Breach, pp. 261–387.

Hartnady, C., Joubert, P. & Stowe, C. (1985). Proterozoic crustal evolution in southwestern Africa. *Episodes* **8**, 236–244.

Iacumin, M. (1998). Studio petrologico, geochimico ed isotopico dei dicchi proterozoici delle serre di Azul e Tandil (provincia di Buenos Aires, Argentina): aspetti petrogenetici ed implicazioni geodinamiche. Ph.D. thesis, University of Trieste.

Ionov, D. A. & Hofmann, A. W. (1995). Nb–Ta-rich mantle amphiboles and micas: implications for subduction-related metasomatic trace element fractionation. *Earth and Planetary Science Letters* **131**, 341–356.

Irvine, T. N. & Baragar, W. R. A. (1971). A guide to the chemical classification of the common volcanic rocks. *Canadian Journal of Earth Sciences* **8**, 523–548.

Kawashita, K., Varela, R., Cingolani, C., Soliani, E., Jr, Linares, E., Valencio, S. A., Ramos, V. A. & Do Campo, M. (1999). Geochronology and chemostratigraphy of 'La Tinta' Neoproterozoic sedimentary rocks, Buenos Aires province, Argentina. *Actas II South American Symposium on Isotope Geology, Cordoba, Argentina*. Cordoba: Subsecreteria de Mineria de la Nacion/Istituto de Geologia y Recursos Minerales/Servicio Geologico Minero Argentino, Annales XXXIV, 403–407.

Kelemen, P. B., Shimizu, N. & Dunn, T. (1993). Relative depletion of niobium in some arc magmas and the continental crust: partitioning of K, Nb, La and Ce during melt/rock reaction in the upper mantle. *Earth and Planetary Science Letters* **120**, 111–134.

Kretz, R. (1982). Transfer and exchange equilibria in a portion of the pyroxene quadrilateral as deduced from natural and experimental data. *Geochimica et Cosmochimica Acta* **46**, 411–421.

Le Bas, M. J., Le Maitre, R. W., Streckeisen, A. & Zanettin, B. (1986). Chemical classification of volcanic rocks based on the total alkali–silica diagram. *Journal of Petrology* **27**, 745–750.

Loucks, R. R. (1996). A precise olivine–augite Mg–Fe-exchange geothermometer. *Contributions to Mineralogy and Petrology* **125**, 140–150.

Ludwig, K. R. (1985). User's manual for 'Analyst', a computer program for control of an Isomas 54E thermal-ionization, single collector mass-spectrometer. *US Geological Survey Open-File Report*, 93 pp.

Macdonald, G. A. & Katsura, T. (1964). Chemical composition of Hawaiian lavas. *Journal of Petrology* **5**, 82–133.

MacGregor, I. D. (1974). The system MgO–Al_2O_3–SiO_2: solubility of Al_2O_3 in enstatite for spinel and garnet peridotite compositions. *American Mineralogist* **59**, 110–119.

Mazzucchelli, M., Rivalenti, G., Piccirillo, E. M., Girardi, V. A. V., Civetta, L. & Petrini, R. (1995). Petrology of Proterozoic mafic dyke swarms of Uruguay and constraints on their mantle source composition. *Precambrian Research* **74**, 177–194.

McKenzie, D. P. & O'Nions, R. K. (1991). Partial melt distributions from inversion of rare earth element concentrations. *Journal of Petrology* **32**, 1021–1091.

Miyashiro, A. (1974). Volcanic rock series in island arcs and active continental margins. *American Journal of Science* **274**, 321–355.

Papike, J. J., Cameron, K. & Baldwin, K. (1974). Amphiboles and pyroxenes: characterization of other than quadrilateral components and estimates of ferric iron from microprobe data. *Geological Society of America Bulletin* **6**, 1053–1054.

Parker, A. J., Rickwood, P. C. & Tucker, D. H. (1990). *Mafic Dykes Emplacement Mechanism*. Rotterdam: A. A. Balkema.

Philips (1994). *X40 Software for XRF analysis. Software Operation Manual*. Eindhoven: Philips.

Ramos, V. A., Leguizamon, A., Kay, S. M. & Teruggi, M. (1990). Evolucion tectonica de las Sierras de Tandil (Provincia de Buenos Aires). San Juan, Argentina. *Actas decimo primer Congreso Geologico Argentino* (2), 311–314.

Rapela, C. W., Dalla Salda, L. H. & Cingolani, C. A. (1974). Un intrusivo basico ordovicico en la 'Formacion La Tinta' (Sierra de los Barrientos, provincia de Buenos Aires, Argentina). *Revista Asociacion Geologica Argentina* **29**, 319–331.

Reid, D. L. (1997). Sm–Nd age and REE geochemistry of Proterozoic arc-related igneous rocks in Richtersveld Subprovince, Namaqua mobile belt, Southern Africa. *Journal of African Earth Sciences* **24**, 621–633.

Reid, D. L., Welke, H. J., Erlank, A. J. & Betton, P. J. (1987). Composition, age and tectonic setting of amphibolites in the central Bushmanland Group, western Namaqua Province, Southern Africa. *Precambrian Research* **36**, 99–126.

Ringwood, A. E. (1966). Composition and origin of the Earth. In: Hurley, P. M. (ed.) *Advances in Earth Science*. Cambridge, MA: MIT Press, pp. 287–356.

Rivalenti, G., Mazzucchelli, M., Molesini, M., Petrini, R., Girardi, V. A. V., Bossi, J. & Campal, N. (1995). Petrology of Late Proterozoic mafic dikes in the Nico Perez region, central Uruguay. *Mineralogy and Petrology* **55**, 239–263.

Rivalenti, G., Mazzucchelli, M., Girardi, V. A. V., Cavazzini, G., Finatti, C., Barbieri, M. A. & Texeira, W. (1998). Petrogenesis of the Paleoproterozoic basalt–andesite–rhyolite dyke association in the Carajas region, Amazonian craton. *Lithos* **43**, 235–265.

Rogers, J. J. W. (1996). A history of continents in the past three billion years. *Journal of Geology* **104**, 91–107.

Ryerson, F. J. & Watson, E. B. (1987). Rutile saturation in magmas: implications for Ti–Nb–Ta depletion in island-arc basalts. *Earth and Planetary Science Letters* **86**, 225–239.

Stormer, J. C. & Nicholls, J. (1978). XLFRAC: a program for interactive testing of magmatic differentiation models. *Computers and Geoscience* **4**, 143–159.

Sun, S. S. & McDonough, W. F. (1989). Chemical and isotopic systematics of oceanic basalts: implications for mantle compositions and processes. In: Saunders, A. D. & Norry, M. J. (eds) *Magmatism in Ocean Basins*. *Geological Society, London, Special Publications* **42**, 313–345.

Takahashi, E. & Kushiro, I. (1983). Melting of a dry peridotite at high pressure and basalt magma genesis. *American Mineralogist* **68**, 859–879.

Takazawa, E., Frey, F., Shimizu, N. & Obata, M. (1996). Evolution of the Horoman Peridotite (Hokkaido, Japan): implications from pyroxene compositions. *Chemical Geology* **134**, 3–26.

Teruggi, M. E., Kilmurray, J., Rapela, C. W. & Dalla Salda, L. (1974). Diques basicos en la Sierra de Tandil. *Revista Asociacion Geologica Argentina* **29**, 41–60.

Teixeira, W., Renne, P., Bossi, J., Campal, N. & D'Argella Filho, M. (1999). ^{40}Ar–^{39}Ar and Rb–Sr geochronology of the Uruguayan dike swarm, Rio de la Plata Craton and implications for Proterozoic intraplate activity in western Gondwana. *Precambrian Research* **93**, 153–180.

Trompette, R. (1994). *Geology of Western Gondwana (2000–500 Ma)*. Rotterdam: A. A. Balkema.

Varela, R., Dalla Salda, L. & Cingolani, C. (1985). La edad Rb–Sr del granito de Vela, Tandil. *Resumen Primeras Jornadas Geologicas Bonaerenses*, 881–890.

Varela, R., Cingolani, C. & Dalla Salda, L. (1988). Geocronologia rubidio–estroncio en granitos del basamento de Tandil, Provincia de Buenos Aires, Argentina. *Actas Segundas Jornadas Geologicas Bonaerenses*, 291–305.

Wilkinson, J. F. G. & Le Maitre, R. W. (1987). Upper mantle amphiboles and micas and TiO_2, K_2O, and P_2O_5 abundances and $100Mg/(Mg + Fe^{2+})$ ratios of common basalts and andesites: implications for modal mantle metasomatism and undepleted mantle compositions. *Journal of Petrology* **28**, 37–73.

Yale, L. B. & Carpenter, S. J. (1998). Large igneous provinces and giant dike swarms: proxies for supercontinent cyclicity and mantle convection. *Earth and Planetary Science Letters* **163**, 109–122.

Zanettin, B. (1984). Proposed new chemical classification of volcanic rocks. *Episodes* **7**, 19–20.